The composite nanomaterials containing (R)-thalidomide-molecularly imprinted polymers as a recognition system for enantioselective-controlled release and targeted drug delivery

Acharee Suksuwan,[1] Luelak Lomlim,[1] Thanyada Rungrotmongkol,[2] Titpawan Nakpheng,[1] Franz L. Dickert,[3] Roongnapa Suedee[1]

[1]Department of Pharmaceutical Chemistry, Faculty of Pharmaceutical Sciences, Molecular Recognition Materials Research Unit, Drug Delivery System Excellence Center, Nanotec-PSU Center of Excellence on Drug Delivery Systems, Prince of Songkla University, Hatyai, Songkhla 90112, Thailand

[2]Department of Biochemistry, Faculty of Science, Chulalongkorn University, 254 Phayathai Road, Bangkok 10330, Thailand

[3]Department of Analytical Chemistry, University of Vienna, Währingerstrasse 38 A-1090, Vienna, Austria

Correspondence to: R. Suedee (E-mail: roongnapa.s@psu.ac.th)

ABSTRACT: A molecularly imprinted polymer (MIP) enantioselective receptor for the (R)-thalidomide enantiomer was synthesized and evaluated for its ability to deliver the drug to cancer cells. Polymer networks with precisely engineered binding sites were built into the assembled nanoparticles by a self-organizing template in the prepolymerized mixture using methacrylic acid, a fluorescently active 2,6-bis(acrylamido)pyridine and N,N' methylene-bis-acrylamide, via both a covalent approach and a physical approach. The fine-tuning of particle diameters was carried out by changes to the polymerizing synthesis method, the type of solvent and the amount of the poloxamer that led to an optimal formulation of the nanoparticles with sizes as small as 100 nm. Data from the ^{1}H-nuclear magnetic resonance spectroscopy revealed the important structural motifs of an (R)-thalidomide-selective cavity for two different polymerization processes. We have investigated their ability for enantiomer recognition and the potential ability to protect the chiral MIP with a self-assembled poloxamer structure. Moreover, the effect of the smaller molecular size can not only enable favorable imaging properties but also facilitate enhanced green fluorescence intensity for the deposited MIP and the (R)-thalidomide in the poloxamer nanoparticles in a cell-line in which the grafted MIP being higher than the deposited one. It was also demonstrated that the deposited MIP nanoparticles had the potential to make the drug effective for attacking multidrug-resistant cells. Thus, the poloxamer nanoparticles containing a thermoresponsive MIP could maximize the release of the nontoxic (R)-thalidomide at the tumor tissue, with the help of a proper temperature shift at the site. © 2015 Wiley Periodicals, Inc. J. Appl. Polym. Sci. **2015**, *132*, 41930.

INTRODUCTION

Natural, biological processes can produce polymers that involve natural building blocks such as amino acid, sugar, and nucleic acid and are assemble into a three-dimensional macromolecular assembly for one particular function from many possibilities. In the past decade, sophisticated macromolecular arrangements in advanced materials have been developed, which show a potential for expanding therapeutics.[1] Molecularly imprinted polymers (MIPs) can reproduce the ability to create template-sensitive cavities from predetermined recognition selectivity for example: for a chiral compound, or for a specific template molecule, or for a physically closely related compound, yet still allow for a target re-inclusion without any chemical interaction with the polymer system. The number of enabling technologies of molecular imprinting have allowed different applications of specific cavities as artificially derived antibodies[2] or an immunoglobulin[3] or for detecting and binding a specific toxin.[4] They may even be of some use for the synthesis of enzyme inhibitors.[5] Our previous studies on the generation of a chiral imprint site has shown that the approach was capable of distinguishing between two enantiomers and provided an opportunity for a chiral drug delivery.[6,7]

A self-organizing system that was capable of fabricating a supra-molecular system had a molecular cavity that involved

preorganization of the polymerizing mixture, which enables complementary counterparts and necessary enantioselective sites to be linked to a self-regulating system. This approach was very attractive, as it was a simple-targeted production of a hydrogel biomaterial containing functional material of an MIP system for use as a recognition element and a signaling function for targeted drug and selective drug delivery. By using an environmentally sensitive system, allowed structural motifs onto the polymeric chains and became self-assembled into the nanoparticle that could lead to a rapid cellular uptake and subsequent enhanced therapeutic efficiency.[8] Within this work, we report the design and synthesis of thermoresponsive MIP nanoparticles selective for (R)-thalidomide, with the use of the functional monomers bearing interactive functional groups, allowing good fit for the model drug (R)-thalidomide as a template in an imprinted cavity. The method based on polymerization process of mixed functional monomers together with a crosslinker and poloxamer to nanoparticles that were capable of having thermo-stimulated responsiveness that led to strong interactions with the target molecule. This approach also yields added benefits including a reduced nonspecific binding and improved transport of the template.

Thalidomide (α-phthalimidoglutarimide) is an inhibitor of angiogenesis and is an efficient inhibitor of tumor necrosis factor-α (TNF-α). It has also been proven to be an efficient antiinflammatory agent in medical therapies such as in cases of severe cutaneous ulceration. Thalidomide was introduced in 1960s as a sedative and hypnotic drug for pregnant women. It was subsequently withdrawn from the market the incidence of severe teratogenicity caused by the (S)-thalidomide enantiomer. The drug has a stereocenter and it is used as a racemate with both the (S)-(−)- and (R)-(+)-enantiomers possessing biological effects for multiple myeloma and related plasma cell disorders in clinical practice.[9] Unfortunately, both thalidomide enantiomers undergo a fast-rate bidirectional chiral inversion in humans.[10] Several thalidomide analogs have been synthesized with their ability to increase the levels of IL-2 that possesses antitumor activity or modulating the immune system for anti-angiogenic activities.[11]

Chiral recognition of a single thalidomide enantiomer by a polymer has been previously reported. In that case it was achieved by the copolymerization of different multifunctional monomers using the method of simultaneous multiple interactions with the template.[12,13] In this current study, chiral recognition by a molecular bis(acrylamido)pyridine-based chirally imprinted polymer and its formation by a self-assembled process have been investigated. A prepolymerized MIP formulation and the macromers were used to generate an engineered binding site complementary with the structure of the (R)-thalidomide that provided self-organization of the macromolecular multicomponent, resulting in the enhanced interfacial regions and surface interactions of the resultant nanoparticles. The functional material having the ability of polymer to have a temperature-controllable mediated transition property was achieved with the fabrication of composite nanomaterials.[14,15] This molecular imprinting technique enabled a chiral entity within the intact assemblies of a polyacrylamide, that had been previously shown to have a double-stimulus property in an aqueous medium,[16] and led to a cooperative response of the nanoparticles.[17] A thermoresponsive polymer made it possible to provide for a thermal stimulus control in their microenvironment by modulation of an interaction of a well-defined recognition system with specific stereoisomers resulting in a significant pharmaceutical action. In addition, the poloxamers consisted of a tri-block copolymer of a poly(ethylene oxide) (PEO) and a poly(propylene oxide) (PPO) block that had shown a high potential for constructing such systems as biomimetic antennae,[18] cell encapsulation and targeting a drug to a tumor cell through micellar nanocarriers.[19] Poloxamers have been found to provide protection of the development of multidrug resistance in breast cancer cells.[20] They were biocompatible, nontoxic with only weak immunogenic properties.[21] The interfacial interactions resulted in the increasing hydrophobic properties to bind to the PPO block, and hence to the generation of an enantioselective interaction site with a high affinity for the (R)-thalidomide in the polymerizing nanoparticles that showed the potential to protect the system and also enhanced the efficiency of the release of the enantiomer from the binding sites. The amount of the added macromer required to prepare the MIP in the polymerizing nanoparticles was optimized and various polymerization methods were determined that would allow for a precise control over the particle size. The tunable monomer template ratio was more favorable to the complexation of the template and the functional monomer during the polymerization process. Thus, the enhancement of supermolecular interactions of the synthesized polymer material can be achieved and that are able to produce selective delivery of a drug of interest at an appropriate receptor site or even DNA in the tumor cells, reducing the needed treatment of anticancer drugs.[22] We have investigated the cellular uptake and cytotoxicity of the (R)-thalidomide loaded MIPs in the adenocarcinoma epithelial cell line (A 549) as a multidrug resistant tumor cell model.

In this manuscript, we described the fabrication of nanosized materials for enantioselective-controlled release by generating polymer recognition material within nanoparticles. The investigation of optimum conditions for the synthesis that was affected the macromeric structures through the method of polymerization was carried out. The morphology and thermal properties of the molecular imprints assembled into poloxamer nanoparticles were examined by using scanning electron microscopy (SEM), confocal laser scanning microscopy (CLSM), thermogravimetric analysis, and transmission electron microscopy (TEM). Investigation of the enantioselective recognition property of both types of imprinted polymers upon rebinding process was also carried out by using the proton nuclear magnetic resonance spectra (^{1}H-NMR). The influences of the parameters (medium pH and temperature) on the chiral recognition properties of the obtained nanoparticles were investigated using batch binding experiments and a diffusion study. Finally, the evaluation of cell uptake of composite nanomaterials was performed to examine the ability for re-binding and the reversible release of the (R)-thalidomide, if the MIPs were immobilized within a cancer cell-line.

Table I. The Composition and Polymerization Processes for (R)-Thalidomide-Imprinted Polymers and the Corresponding Nonimprinted Polymers for Both Polymerization Processes

Polymer	(R)-Thalidomide (template) (mmol)	MAA (mmol)	BAAP (mmol)	MBAA (mmol)	Poloxamer (mmol)	Acrylate poloxamer (mmol)	AIBN (mmol)	Porogen (mL)
Deposited MIP	0.035	0.070	0.070	0.320	0.008	–	0.050	5
Deposited NIP	–	0.070	0.070	0.320	0.008	–	0.050	5
Grafted MIP	0.035	0.070	0.070	0.320	–	0.008	0.050	5
Grafted NIP	–	0.070	0.070	0.320	–	0.008	0.050	5

EXPERIMENTAL

Materials

($+$)-(R)-Thalidomide (98.0%), ($-$)-(S)-thalidomide enantiomers (99.0%), ($\pm$)-(rac)-thalidomide (99.0%), methacrylic acid (MAA), triethylamine, and 2,6-diaminopyridine were from Sigma-Aldrich (St. Louis, MO); 2,2′-azobis(2-methylbutyronitrile) (AIBN) from Janssen (Geel, Belgium); acryloyl chloride, N,N'-methylene-bis-acrylamide (MBAA) analytical grade, and Pluronic® F127 (poloxamer 407, cell culture-tested grade, Mw ~10,000 Da) from Fluka (Buchs, Switzerland); MeOH-d$_4$ (99.8%) from Wilmad-LabGlass (Vineland, NJ); and the acetic acid-d$_4$ (99.5%) from Cambridge Isotope Laboratories (Andover, MA). MAA was purified by distillation under reduced pressure, and 2,6-diaminopyridine was recrystallized from benzene before use. All other solvents were obtained from Labscan (Dublin, Ireland), and were of either analytical reagent grade or HPLC grade, and were used as received. Working standard solutions were prepared daily.

Synthesis of 2,6-bis(acrylamido)pyridine

The synthesis of BAAP was adapted from the method of Oikawa et al.,[23] with a slight modification. One gram of 2,6-diaminopyridine (10 mmol) and triethylamine (2.53 g, 25 mmol) were dissolved in dry tetrahydrofuran (60 mL). Acryloyl chloride (1.99 g, 22 mmol) was gradually dropped into the solution at 0°C. The reaction mixture was continuously stirred at 4°C in a nitrogen atmosphere. After 2 h, 10 mL of distilled water was added to this mixture. The white precipitates were extracted with two portions of 50 mL of chloroform. The organic layers were combined, washed with saturated sodium carbonate, then water, and dried in vacuo. The crude solid was recrystallized from benzene to yield 2,6-bis(acrylamido)pyridine (61%) as a pale yellow solid (mp = 151–154°C): IR (KBr) d 3327 cm^{-1} (v_{N-H}), 1700 cm^{-1} ($v_{C=O}$), and 1680 cm^{-1} ($v_{C=C}$); ^{1}H-NMR (DMSO-d$_6$, 500 MHz) d 5.6–6.8 ppm (m, 6H, 2CH=CH_2), 7.8–8.0 ppm (m, 3H, pyridine ring), and 10.3 ppm (s, 2H, 2NHCO); MS m/z: 216.19. Subsequent analysis calculated for $C_{11}H_{11}N_3O_2$: C, 60.82; H, 5.10; N, 19.35. The following results were revealed: C, 61.24; H, 4.64; N, 18.05.

Synthesis of a Functionalized Acrylate Poloxamer

Poloxamer 407 (6 g, 0.73 mmol) and triethylamine (0.30 g, 2.94 mmol) were added in dry tetrahydrofuran (60 mL); acryloyl chloride (0.27 g, 2.94 mmol) was then added into the mixture in drops and stirred vigorously at 0°C in a nitrogen atmosphere. The reaction mixture was stirred for 3 h at 4°C, then was left at

room temperature overnight. The triethylammonium chloride formed was quenched with 10 mL of MeOH; the product was filtered and concentrated under reduced pressure. The degree of substitution, which was calculated from the ratio of the area of the methyl peak to the vinyl peak of the NMR spectrum, was ~90%. The product was purified in an excess amount of diethyl ether to yield the diacrylate poloxamer (85%) as a deep yellow oil: IR (KBr) d 2891 cm^{-1} (v_{C-H}), 1729 cm^{-1} ($v_{C=O}$), 1636 cm^{-1} ($v_{C=C}$), and 1113 cm^{-1} (v_{C-O-C}); ^{1}H-NMR (D$_2$O, 500 MHz) d 1.19 ppm (s, 3H, –CH_3), 4.3 ppm (t, 4H, –CH$_2$–CH_2–O–), 6.15 ppm (dd, 2H, CH$_2$=CH–COO–), and 5.90–6.40 ppm (d, 4H, CH_2=CH–COO–); from gel permeation chromatography (MeOH), the calculated M_w was 11,093 ($M_w/M_n = 1.04$).

Preparation of (R)-Thalidomide Molecularly Imprinted Polymers

The molecularly imprinted polymer nanoparticles were produced through a free radical-initiated mechanism with the macromer (poloxamer or diacrylate poloxamer) and other polymeric compositions for the MIP formulation, as shown in Table I. The prepolymerization mixture was then degassed in an ultrasonic bath for 10 s, and bottles were sealed in a nitrogen atmosphere. The polymerization reaction was allowed to proceed for 10 h under the polymerization protocols with or without sonication. Subsequently, the resultant nanoparticles were washed three times with 400 mL of cool MeOH and a 1 : 9 (v/v) acetic acid and MeOH mixture, followed by a dialysis using a CelluSep T2 membrane with a cutoff of 8000 Da (Interchim, Montlucon, France). The nonimprinted control polymer that was used to determine the enantioselectivity of the imprinting polymer was prepared by the same procedure except there was no template.

Characterizations of the Polymer Nanoparticles

The molecular sites the chirally imprinted cavities were characterized by several different methods. TEM images of the obtained nanoparticles were analyzed using a JEOL JEM-2010 transmission electron microscope (JEOL, Germany). Confocal laser scanning microscopy (CLSM) was used to investigate the physical structure of the imprinted sites for the nanoparticles. An LSM 700 (Zeiss, Oberkochen, Germany) was used, equipped with an X-Cite 120 lamp/HBO 100 mercury lamp and a 40× dry objective lens. The fluorescent intensity of the BAAP monomer into the polymer matrix was measured using ZEN 2009 software (Zeiss) within a 1-μm radius of the polymer surface ($n = 20$). In addition, the particle size distribution of the nanoparticles was examined using an LS230 laser particle size

analyzer (Beckman Coulter, Brea, CA) at a fixed scattering angle of 90°. Thermogravimetric analysis of the imprinted nanoparticles was performed using a Perkin Elmer TGA-7 thermogravimetric analyzer (Perkin Elmer, MA) at a heating rate of 10°C min^{-1} under a stream of nitrogen gas at 50 mL min^{-1}. In addition, the elemental composition of the nanoparticles was examined with a JEOL electron microscope and a microanalysis system (Oxford Instruments Link-ISIS 300). The ^{1}H-NMR spectra and the NOE difference were recorded on a Varian INOVA 500 NMR spectrometer (Varian, Unity, UK) in 2 mL of MeOH-d$_4$ during the polymerization processes at various time intervals, and this was followed by the addition of acetic acid-d$_4$, using TMS as the internal standard. A two-dimensional excitation–emission fluorescence matrix (2D-FEEM) spectroscope was used to map the fluorescent surface of the obtained nanoparticles using an FP-6200 spectrometer equipped with a 150-W xenon lamp and 10 mm quartz cells. Analytes (0.05 mg mL^{-1}) were scanned at 30 nm s^{-1} in a 1-cm quartz cuvette at room temperature (25°C).

Determination of the Desorption in Various Solvent Media

The complexation studies of the MIP nanoparticles with enantiomers were performed in various medium conditions: phosphate buffers pH 5.5, 7.4, or 8.0, and 27°C, 37°C, or 45°C in 0.1 M phosphate buffer (pH 7.4). A control experiment was carried out using a nonimprinted reference polymer (NIP). Samples composed of weighed amounts of polymers (5 mg) were added to 5 mL of a solution containing 0.25–0.75 μg mL^{-1} of the racemic mixture or 1 μg mL^{-1} of the individual thalidomide enantiomer, and mixtures of the (R)- and (S)-thalidomide (3 : 1, 1 : 3, and 1 : 1). The solution was stirred overnight to establish equilibrium. The suspensions of the solid particles were centrifuged (4000g, 4°C), and an aliquot was immediately taken. The amounts of enantiomers in the samples of the incubation medium were immediately analyzed using a stereospecific HPLC method as below. The samples were fast-chilled and stored at −20°C before analysis.[24] A mean value from three determinations was obtained and recorded.

Evaluation of Enantioselective Release

A drug-polymer ratio of 4 : 1 in an aqueous solution (10 mL) was applied to the chloroform organic layer (10 mL) along with a magnetic bar (100 rpm) in the U-tube with an exposed surface area of 0.78 cm^2 after equilibration (15 min), and delivery into a pH 5.5 buffer receiving phase (10 mL) was at 42°C. At fixed time intervals, 500 μL samples were withdrawn for the analysis of the enantiomers by stereospecific HPLC as described below, and the external aqueous phase was replaced with a fresh buffer solution. The data were processed using nonlinear regression to a standard sigmoidal dose–response curve to obtain the IC_{50} value, which was the amount that produced 50% of the maximum response; this was a simple measure of the potency. In this case, the IC_{50} was examined from the concentration of each enantiomer from the polymer that penetrated 50% into the receiving medium of the U-tube.

An enantiomer-specific assay for the thalidomide enantiomers in the dissolution samples was carried out by stereospecific HPLC using a chiral HPLC column. HPLC assays were performed by injecting a 20-μL sample onto a 150 mm × 4.0 mm Chiral-CBH column (Chrom Tech, MN), with a mobile phase of 10 mM phosphate buffer (pH 5.5) containing 50 mM disodium EDTA and 2% (v/v) acetonitrile operating at a flow rate of 1 mL min^{-1}. A Waters 600 HPLC system with a Waters 717 plus autosampler, equipped with Waters 486 variable wavelength UV detector operating at 225 nm, and a Waters 746 integrator was used (Bedford, MA). The validation of the analytical method was conducted according to the standard protocol.[25] The correlation coefficients for the calibration curves were in the concentration range of 0.05–5 μg mL^{-1} for the (R)- and (S)-thalidomide enantiomers ($n = 6$) and were greater than 0.997. The limit of detection (LOD) was 0.02 μg mL^{-1}, and the percentage recovery was in the range of 95–105%, with an RSD of less than 2% ($n = 15$).

Biological Trial for Drug Delivery

The cancer cells were grown in a culture medium to a density of 1.2×10^5 cells cm^{-2} in 24-well ImageLock plates (Essen Instruments, MI) and were used when they had formed confluent monolayers. The obtained nanoparticles were incubated with the thalidomide methanol solution (20 mg mL^{-1}) overnight, and evaporation was then conducted after the washing of nonabsorbed thalidomide nanoparticles by methanol solvent, before inspection by microscopic isotropy using a polarized microscope (Leica, Hamburg, Germany). In addition, the tapping mode imaging of the test nanoparticle was run with a Veeco Atomic Force Microscope (Digital Instruments Nanoscope IIIa, CA). In the case of drug loading, the deposited or grafted nanoparticles were incubated overnight with (rac)-thalidomide solution (125 μg mL^{-1} in methanol) and then dried under vacuum. Subsequently, confocal microscopic images were obtained after placing the plates in the Incucyte chamber in an atmosphere of 5% CO$_2$, and cells were left to attach at 37°C for 3, 24, and 28 h after drug treatment was carried out. The quality of the successful assay was confirmed by a coefficient of variation of less than 15% in the blank cell (control). Every experiment was carried out three times. Furthermore, the nanocarriers (500 μg mL^{-1}) containing the drug were reconstituted in phosphate buffered saline pH 7.4 and sterile-filtered through a membrane with a 0.20 μm pore size before assessing the drug activity in the cells. The cells cultured before and after incubation with the test nanoparticles were photographed on a *Nikon Eclipse TE 2000-V* inverted *microscope* (Nikon, Tokyo, Japan) with or without excitation using UV when the emission was monitored at 525 nm. All data were calculated and presented as a mean value ± SD. The paired *t*-test compared the green fluorescent intensities before and after the cell uptake study.

Molecular Modeling

The structures of the MIPs and the optimized topology of the molecules were generated with the Material Studio (MS) program version 6.0 (Accelrys, CA), GaussianView 5.0 software, and the Gaussian 03W program. The study on the contribution of the MIP to the poloxamer structure was performed by a molecular dynamic (MD) simulation of the annealing module for both types of imprinted polymers. The selective material had a MW of about 29,000 g mol^{-1}, and the poloxamer side chain was heated to 500 K and cooled down at 10 K for 50
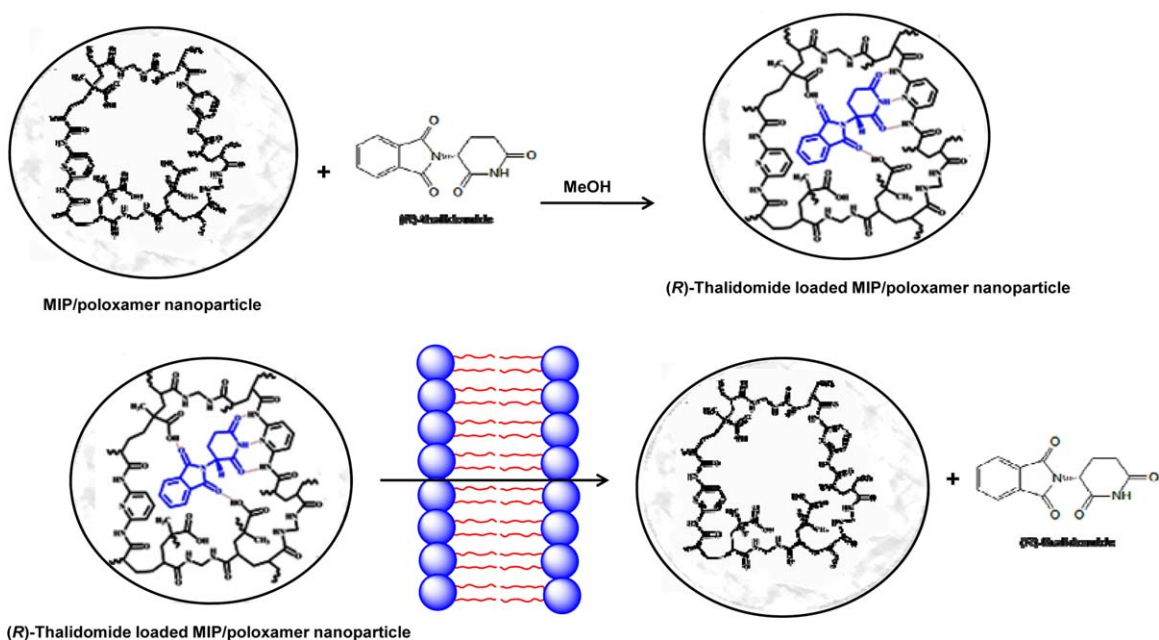
Figure 1. Schematic representation of the process of drug release from (R)-thalidomide-molecularly imprinted polymers in the poloxamer nanoparticles can kill cancer cells. [Color figure can be viewed in the online issue, which is available at wileyonlinelibrary.com.]

cycles. Subsequent experiments with the optimal structure of the respective MIP template complexes that contained 17,193 g mol^{-1} of MIP and 12,000 g mol^{-1} of poloxamer were carried out. The molecular dynamic simulation was performed for a constant volume/constant-temperature ensemble (NVT) at a temperature range of 298–318 K in MeOH. The geometrical optimizations were performed at the B3LYP/6–311++(d,p) level, and a time step of 1.0 fs was used, with a total simulation time of 1500 fs. The temperature was maintained using an Andersen thermostat with a collision ratio of 1.0. As applied in the Materials Studio, the Compass was determined as the most suitable force field in all simulations.

RESULTS AND DISCUSSION

The Preparation and Characteristics of the MIP Nanoparticles

The designed MIP in the confined nanoparticles was expected to rebind the desired enantiomer by exposing a large area of the affinity surface to an aqueous solution, which enabled a reversible and selective inclusion of any subsequently added original template. It also provided a response to a change in the environment that resulted in a release of the bound template within the cavity into the receiving medium. Based on the experiment evaluation and data, the scheme of the binding process and the release is proposed. Schematic illustration of the binding process and the release of the enantiomers of thalidomide is shown in Figure 1. Two different templating strategies were used to obtain the imprinted polymer surfaces on the confined nanomaterials, due to noncovalent interactions such as hydrophobic, van der Waals interactions, and hydrogen bondings. The first strategy was from the inclusion domains, while the second was via the formation of a polymeric chain networks by grafting on the molecular architecture of the polymer system. As Supporting

Information, Figure S1 shows the schematic illustration of the formation of an (R)-thalidomide-selective cavity on the imprinted polymer incorporated into the polymeric crosslinked chain within the poloxamer nanoparticles.

The interactions of a series of these composite materials that consisted of different polymerizing MIP compositions, the presence of the poloxamer or the functionalized acrylate poloxamer, and precise control over the size were investigated through monitoring by the laser particle size analyzer. These synthesized polymers were subjected to either photochemical or thermally generated polymerization under sonication or without sonication and to a fixed amount of the macromer at 8 μmol. The photochemical reaction produced a large particle size for the imprinted products (1.1–1.2 μm) at a low temperature and in particular by using MeOH as the porogenic solvent (sees Supporting Information S2). In the nonpolar solvent, the physically immobilized poloxamer MIPs produced a remarkable decrease in the particle dimensions, while allowing for the same particle size in all the 25°C and 60°C cases. However, the sizes of the nanoparticles formed in the MeOH noticeably decreased when the nanoparticles were formed photochemically at 60°C. Meanwhile, a smaller amount of the macromer treated with the reaction mixture produced fewer differences in the particle size to those of the deposited MIP nanoparticles than for the grafted MIP nanoparticles. The particle sizes of the blank poloxamer nanoparticle were found to be about 100 nm and for the poloxamer concentrations of between 2 μmol and 8 μmol, it was 200 nm. The results of particle size measurements indicated that the highest amount of macromer (8 μmol) favored the formation of nanoparticles with the smallest sized nanoparticles of 60 nm. Accordingly, all the cases of the manufactured MIP nanoparticles that will be discussed in the following sections came from the procedures of the synthesis of composite
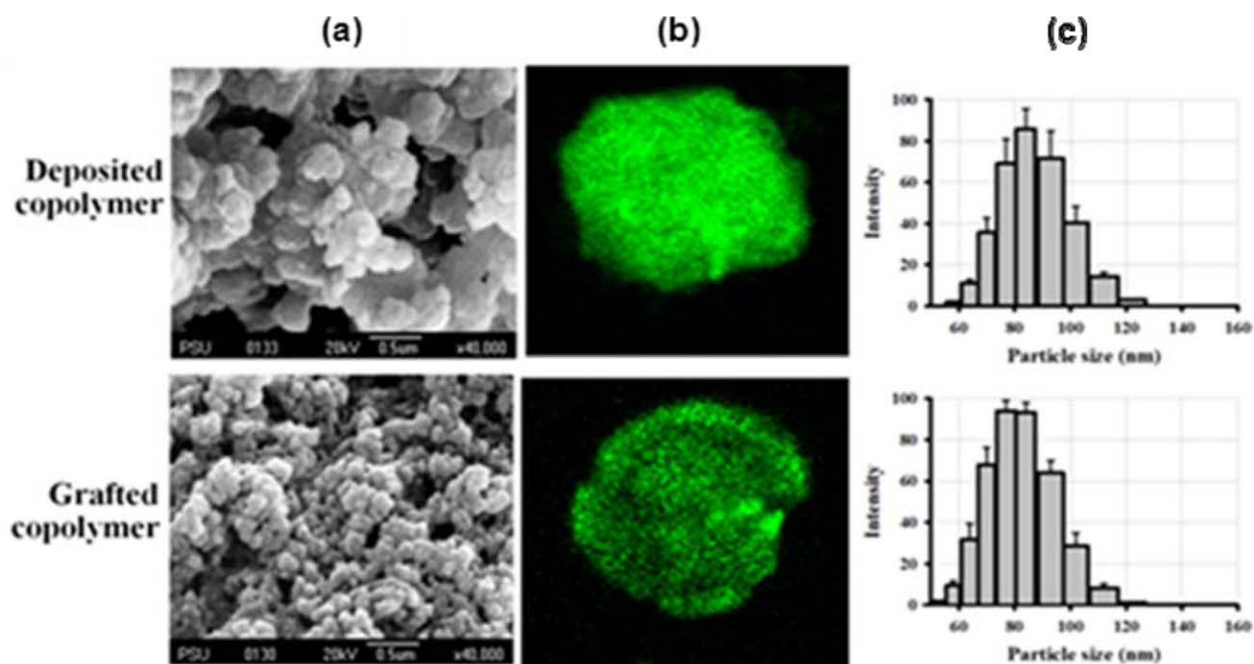
Figure 2. Characterization of the MIP by both the deposit and grafting methods. (a) SEM, (b) CLSM images, and (c) the particle size distribution of the MIP nanoparticles. [Color figure can be viewed in the online issue, which is available at wileyonlinelibrary.com.]

nanomaterials conducted under thermally controlled reaction conditions and methanol as a porogen.

The SEM images of the prepared MIP particles were analyzed (JEOL, Tokyo, Japan), and these showed dense aggregations with bigger ranges of aggregate sizes from both polymerization methods [see Figure 2(a)]. The different polymerization processes led to confined surface structures and spaces within the assembled nanoparticles that could be distinguished from the CLSM images [Figure 2(b)]. In addition, the analysis of the topographic CLSM images revealed an average number of approximately 27% for the MIP that was grafted onto the polymeric chains, whereas for the most intense in the CLSM of the deposited MIP matrix it was 78%. Moreover, the grafting polymerization method yielded a precise particle size of the nanoparticles, while a wide range of size distribution of the nanoparticles was formed by the deposit method [Figure 2(c)].

The pore diameter, pore volume, and BET surface area of imprinted and nonimprinted polymers were inspected by the nitrogen adsorption/desorption techniques. The data given (Table II) indicated that the pore volume and BET surface area of the imprinted polymers were much different from those of the control polymers. Both grafted MIP and NIP showed comparable values for their total pore volume which was much smaller than those of the deposited MIP and NIP. Conversely, the observed differences in the total BET surface area of the grafted MIP showed an approximately twofold larger total surface area than that of the corresponding NIP, but exhibited a smaller surface area than both the deposited MIP and the NIP. Smaller pore dimensions of the grafted MIP and therefore a larger BET surface area could be expected to generate a better size-selectivity of the cavities that enabled a well-defined site for

the template compared to the deposited material. The deposited MIP had the largest pore diameter, while the corresponding NIP contained a fourfold smaller pore size. This indicated that this imprinted polymer could provide a higher number of accessible binding groups with potentially higher binding capacities.

The formation of the thermoresponsive MIP nanoparticles was related to the significant phase transition changes. The LCST was defined as the temperature at which the optical transmittance of the copolymer solution was 50% of the maximum value. That the poloxamer acted as a reference for its thermo sensitivity at temperatures near to those of the human body is well known. These thermoresponsive MIPs, with three-dimensional cross-linked networks created by immobilized colloidal particles assembled from the poloxamer nanoparticles by the grafting and the deposit methods were 38°C and 41°C, respectively, as compared to their parent macromers (i.e., the LCST values for diacrylate poloxamer and poloxamer that were

Table II. Pore Size Analysis of MIPs and NIPs for Both Polymerization Processes

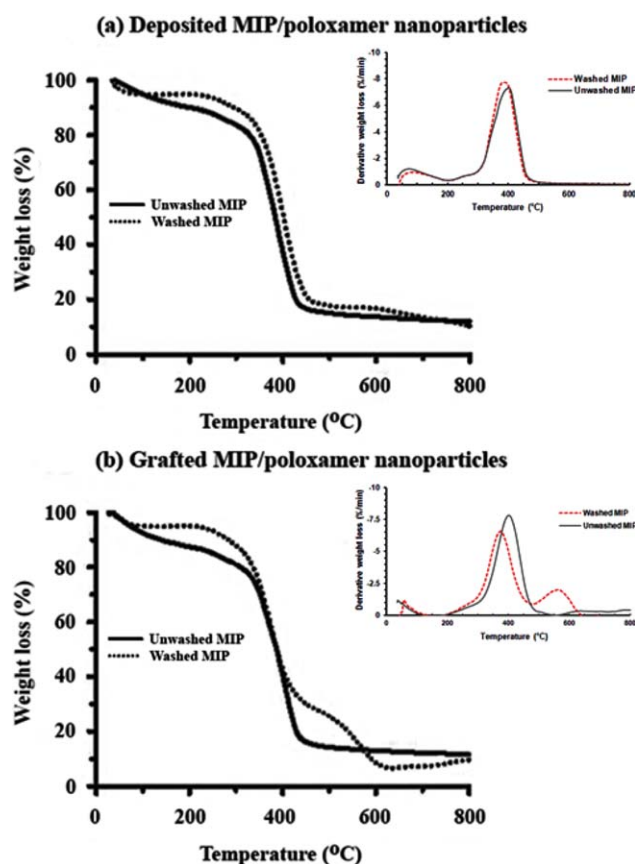| Polymer	Total pore volume (cm^3 g^{-1})	Multipoint BET (m^2 g^{-1})	Total pore diameter (Å)
Deposited MIP	0.2108	43.75	192.80
Deposited NIP	0.0746	60.82	49.04
Grafted MIP	0.7251	226.70	128.00
Grafted NIP	0.3501	109.10	128.30

Figure 3. Thermal gravimetric curves of the MIP/poloxamer nanoparticles produced by (a) the deposit and (b) the grafting method (insert: derivative thermal gravimetric curves of the MIP/poloxamer nanoparticles before and after washing out the templates). [Color figure can be viewed in the online issue, which is available at wileyonlinelibrary.com.]

32°C and 37°C, respectively). We also examined the chemical composition of the obtained MIP nanoparticles, where there was an incorporation of 12.35 mol % of the functional monomers to the binding site, with the amount of the nonfunctional BAAP and MAA being reduced to ca. 9.51 mol % and 11.58 mol %, respectively. This was compared to the 6.53 mol % of the two functional monomers that allowed ligands into the binding site and the remaining bulk polymers that had 1.3 mol % of BAAP and 7.62 mol % of MAA in the grafted materials.

Thermal Behavior and Morphological Properties of the MIP/ Poloxamer Nanoparticles
We have examined the thermal behavior and morphological properties of both types of MIPs that were embedded in the poloxamer using thermal gravimetric analysis and transmission electron microscopy. Figure 3(a) shows the thermal stability of the washed MIPs obtained by the deposit method that was similar to the unwashed one except, there was a slight increase in the weight loss value of the washed MIP material observed at temperatures above a room temperature of up to 50°C. For the grafted MIP material the thermal stability of the altered nanoparticles, showed a slow weight loss of solid at approximately 7 wt % for the washed MIPs. In contrast the unwashed MIPs,

observed at a lower temperature ($<70°C$), had a gradual decrease in mass loss of up to 10% at 250°C [see Figure 3(b)]. We found that the losses of mass in the washed MIPs obtained by the grafting method were actually lower than the mass loss of the unwashed samples and this reduced the thermal stability. A greater amount of the solid weight of the unwashed MIP was lost at temperatures beyond 400°C, while there was a lower weight loss in the case of the washed MIP from the deposited method that was similar to that for the unwashed one [see Figure 3(a)]. The derivative weight loss curves for both the MIPs [Figures 3(a,b), insert] had a maximum decomposition temperature (T_{max}) of approximately 400°C for both the MIP materials. In addition, the washed MIP that was produced by the grafting method had two distinct stages of thermal decomposition one in the range of 200–550°C and the other from 550°C to 600°C with a lower differential peak as compared to the unwashed material [Figure 3(b), insert]. This reduced thermal decomposition of the washed material was perhaps a result of the decreased water content in the MIP/poloxamer nanoparticles. The second thermal decomposition stage occurred at 580°C for the grafted MIP after washing, which indicated that the thermal decomposition of the polymer matrix differed from that of the deposited one and showed no second peak of thermal decomposition [Figure 3(a), insert]. We examined the morphological properties for both the MIP materials by using TEM, as this allowed for a better understanding of the MIP/poloxamer nanoparticles at the microscopic level [see Figure 4(a,b)]. This showed that there was a high interaction of interfacial contact between the deposited MIP and the poloxamer on the separation of the microphase of the mesoporous nanostructure; they showed a facet of grain structure with small 5–nm dark spots and a bright annular shell [Figure 4(a)]. This result indicated a barrier effect that hindered the evaporation of the volatile degradation products of decomposition of the former MIP/poloxamer nanoparticle. The TEM images showed that the resulting flexible nanoparticles had a high density of grafted chains in the poloxamer structure, but no microphase separation of the MIP in the poloxamer nanoparticles was observed. When the MIP became evenly opaque, it was likely that the narrowed optical gap led to the optically inactive dark state of the excitation energy.[26] This can be attributed to the chiral molecular imprinted polymer at its lowest excitation energy having a highly symmetrical geometry of the diamidopyridines. This was in contrast to the former case, for process in which chemicals were physically adsorbed and caused a reduction in their geometric symmetry in conjunction with the realignment of their optical energies, however confirmation of the dark spots will require further spectroscopic experiments. The TEM results demonstrated that they could form self-assembled nanostructures with a strong electron scattering of the chiral molecular imprinted polymer in the structure.

Investigation of the Mechanisms of Chiral Recognition
The use of MeOH as the porogenic solvent was of interest because it also enabled the solubility of the template. However, a large excess of MeOH would prevent the formation of the prepolymer complex during the polymerization process, which was necessary for obtaining an efficient imprinting. The use of
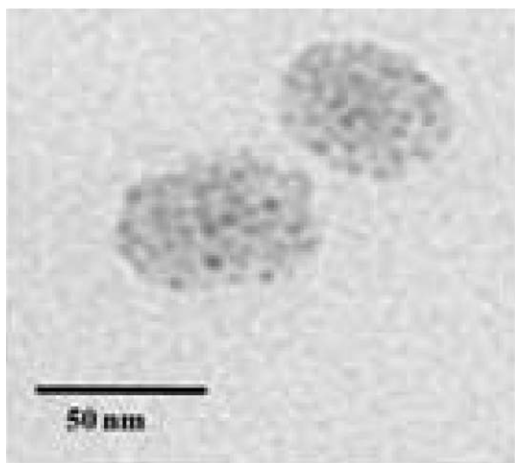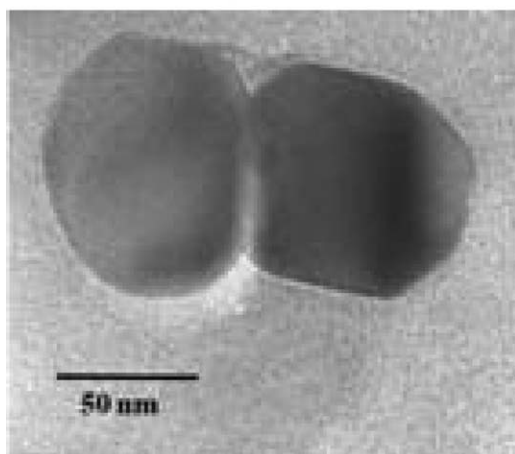
Figure 4. A transmission electron microscopy of the MIP produced by (a) the deposit and (b) the grafting methods.

MeOH was an attempt to exploit the approach of inducing a large-scale cooperative structure of the MBAA-bound MIP.[27] However, we needed to examine the effect of the MeOH solvent on the enantioselective recognition by this MIP system during the templating and polymerization processes using the ¹H-NMR solution method. The ¹H-NMR spectra showed a down field shift of both the 3-methine proton resonances of the template (0.05 ppm) compared to the thalidomide alone at 5.12–5.20 ppm and a slight downfield shift of the aromatic protons on the thalidomide as well as some of the resolved peaks of the BAAP between 7.75 ppm and 7.95 ppm for the deposit polymerization at 15 min [see Figure 5(A)]. So, the self-assembly between the monomers and the template was able to form hydrogen bonds. In addition, the NMR spectra achieved from the deposited polymerization was able to distinguish between the BAAP-crosslinked monomers after the prepolymerization at time zero and beyond 15 min. It is believed that this was due to a different alignment in the diamidopyridine-based chiral molecule that had been imprinted into a sensitive host constructed poloxamer structure. Formation of a tight wrap around the

template in the synthesized polymer product seemed to prevent the template from racemization and degradation into a stimulus-sensitive material. The results indicated that the self-organizing template in the prepolymer mixture exhibited a strong and highly enantioselective binding of the template molecule with methanol as the porogenic solvent that confirmed the presence of a favorable chiral recognition site in a polar protic environment during the polymerization process. In contrast, at 30 min or 45 min, the four separate signals of the methine doublet of doublets had moved (0.05 ppm) with respect to the thalidomide alone (at 5.12–5.20 ppm), and yielded the resolved peak compared to a single peak of the BAAP proton resonances when the polymerization reaction was held at 60°C. Hence, a higher temperature resulted in the template becoming unbound from the binding site of the cross-linked polymer matrix and induced geometries that were unfavorable for any hydrogen-bonding interactions to the template to become embedded into the selective pattern of the imprinted species. This process of the shift in the ¹H-NMR spectra can be explained by the complementivity between the functional groups of the BAAP and MAA, which allowed for a sufficient NH proton coverage towards the center of the binding pocket and created more stable cavities that then exerted a highly desirable effect through orientation of the template inside the cavity. The ¹H-NMR spectra between 15 min, 30/45 min, and 120 min, showed that the potential binding site cavity interacted with the (R)-thalidomide. The subsequent addition of the acetic acid-d₄ showed that the (R)-thalidomide can be regarded as being encaged within the polymer obtained by the deposit method, which resulted in a restriction for an easy dissociation in an acetic acid solution [see Figure 5(A)]. These results indicated that the release of the bound template in the MIP was mainly determined by the BAAP in the polymer: the bonding between the phthalimide moiety of the (R)-thalidomide to the pyridine of the functional monomer, changes the orientation that entails the system of π electrons parallel to the aromatic ring. In the temperature stimulus, it enhanced the transfer of the bound template within the imprinted cavity of the polymer matrix that could provide diffusion of the template by this MIP system.

For the grafted polymerization method, in Figure 5(B), the resolved peaks of the BAAP at 7.75–7.78 ppm instead of a single peak, as was the case for the deposited polymerization, also behaved similarly throughout the synthetic process for 120 min. We found that there was an upfield shift of the chiral 3-methine proton at 5.20 ppm for 0.05 ppm in the ¹H-NMR spectra compared to the thalidomide alone (at 5.12–5.20 ppm) and there was a similar observation for the deposited one. It was of interest, that after adding the acetic acid-d₄ the BAAP and the methine and aromatic protons of the template on the ¹H-NMR of the MIP-grafted polymer moved to down-field and likewise the deposited MIP at 15 min, and this was reflected in the alteration of the signal proton resonances in the template-monomer assembly in the MeOH-d₄, as shown in Figure 5(B). In fact, the addition of acetic acid had a strong impact on the formation of H-bonds, and thereby the formation of a dissociated template-functional monomer complex. In our opinion this indicates the
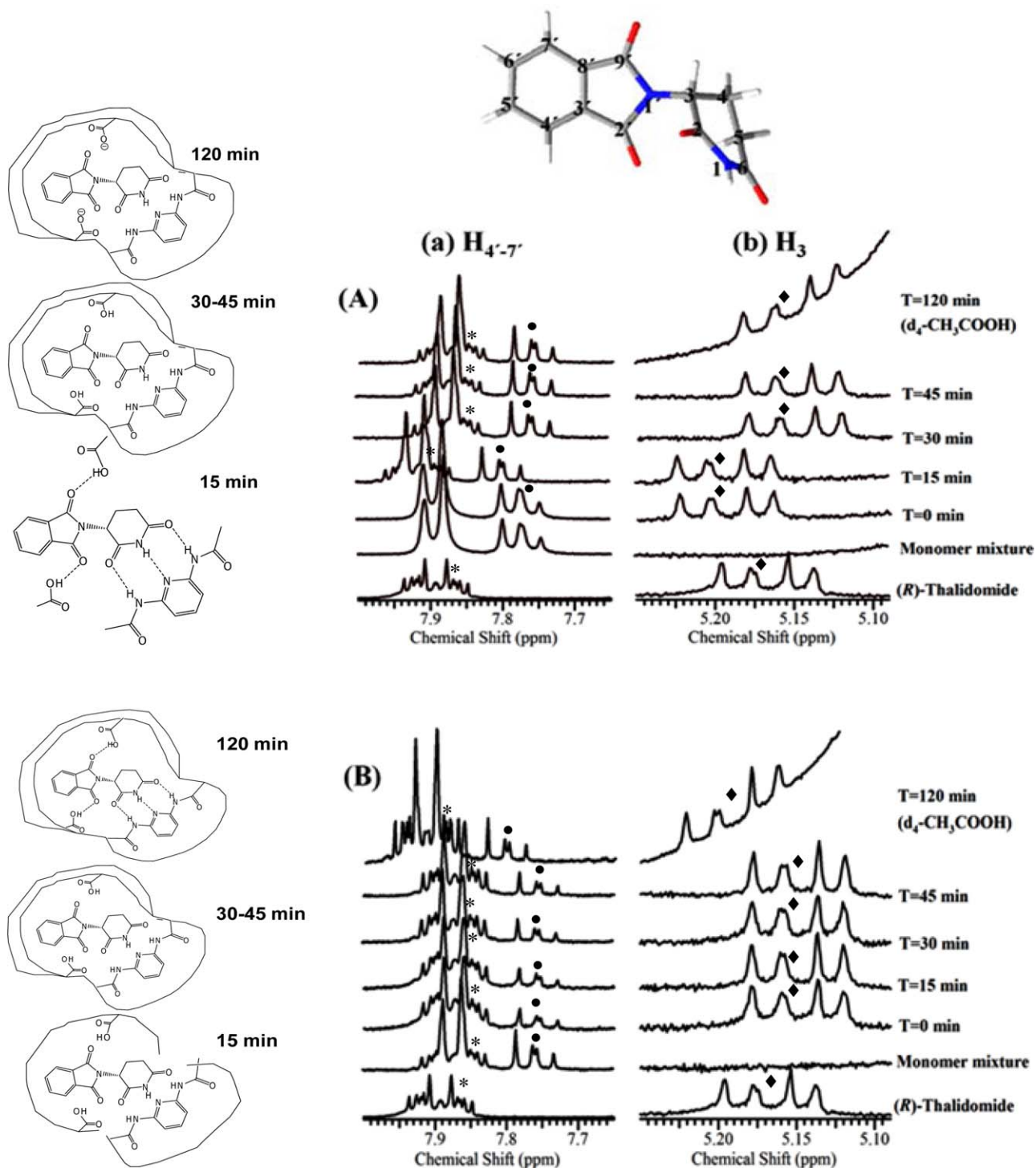
Figure 5. ^{1}H-NMR spectra of a selected region of the (R)-thalidomide enantiomer in the prepolymerized mixture during the polymerization process by (A) the deposit and (B) the grafting method, and with added d$_4$-acetic acid after polymerization and the process of the peaks shifting. * = H$_{4'-7'}$ of thalidomide, • = BAAP, and ◆ = H$_3$ of thalidomide. [Color figure can be viewed in the online issue, which is available at wileyonlinelibrary.com.]

possibility of having an immobilized template in the MIP on the acyl chains of the block copolymer. It was anticipated that the functional monomer preferred to lie in the most favorable conformation that existed for the lone pair electron on the nitrogen to provide a stabilizing effect on the geometry for the template molecule in the polymer matrix.

Furthermore, the intermolecular Nuclear Overhauser Enhancement (NOE) spectra confirmed that the binding sites of the MIP tended to incorporate the templated enantiomer, while at the same time rendering the sites inaccessible to interference by the (S)-isomer (see Supporting Information, Figure S3). The NOE can provide the possibility of studying the movement of

Table III. ^{1}H-NMR Data Showing Saturation Shifts $\Delta\delta_{max}$ (ppm) for the Aromatic and Chiral CH Protons of Thalidomide Enantiomers in MeOH-d$_4$

Polymer	Compound	$\Delta\delta_{max}$ (ppm)[a]			
		Aromatic protons		3-Methine proton	
		27°C	60°C	27°C	60°C
Deposited MIP	(R)-Thalidomide	0.025	0.040	0.030	0.040
	(S)-Thalidomide	0.002	0.001	0.005	0.003
Grafted MIP	(R)-Thalidomide	0.015	0.002	0.015	0.002
	(S)-Thalidomide	0.003	0.002	0.005	0.002

[a] Positive value indicates a downfield shift. (mean ± SD, $n = 3$).

nuclei through space by measurement of their local proximity (Supporting Information, Figure S4). The irradiation of the methyl proton signal of MAA established a strong interaction with the 3-methine proton of (R)-thalidomide at 5.15–5.25 ppm due to the proximity of the two signals. Also the NOE difference spectra revealed a strong enhancement of the 3-methine proton of (R)-thalidomide when the MIP was generated at a ratio of 1 part (R)-thalidomide to two parts of the imprinted polymer (or the 1 : 1 : 1 template/BAAP/MAA), which was the same as the 1 : 4 ratio (or 1 : 2 : 2 template/BAAP/MAA). A weaker NOE effect was found for an excess mixture at a 1 : 8 molar ratio (or 1 : 4 : 4 template/BAAP/MAA) that reduced the absorption peak (30%) with respect to the 1 : 4 mixture for the deposited polymerization method only, as shown in Supporting Information, Figure S4. These results suggest an inherent disorder associated with the surrounding crosslinking chains on each component of the polymers due to increased motion at higher temperatures. In addition, the spatial arrangement of the binding sites in the cavity that involved the intermolecular interactions of the complementary functionality between the template and MIP and the deposited materials should have been different from the grafting polymerization.

Furthermore, the effects of temperature on the adsorption process of the imprinted sites were examined when the template enantiomer was rebinding and the opposite enantiomer by ^{1}H-NMR spectroscopy at 27°C, 37°C, and 60°C using MeOH-d$_4$ as the solvent for both polymers (Table III). When the template enantiomer was added to a solution of the deposited MIP this produced a more significant downfield shift in the aromatic proton (H4′-H7′) of the phthalimide ring ($\Delta\delta \geq 0.15$ ppm) and the stereogenic center ($\Delta\delta = 0.01$–0.012 ppm) of the proton signal. These significant shifts for the (R)-thalidomide were far superior to those for the nontemplated (S)-thalidomide and they operated to a much greater extent than those of the corresponding NIP. In comparison to the binding with the grafted-MIP, the aromatic proton signal and the methine proton (H3) signal shifted for both enantiomers of thalidomide, which were similar at about 0.01 ppm in the presence of the MIP. These could be interpreted as indications of the interactions of both the aromatic protons and the chiral methine proton of the (R)-

thalidomide template enantiomer with the MIPs. The structure and dynamic properties of the MIP during the polymerization process were studied by molecular modeling (see Supporting Information, Figures S5–S7). In addition, the results indicated that it was not only the nature of both the hydrophilic and hydrophobic parts of the nanomaterials, but also the two types of composite nanomaterial was important for reversible binding at spatial defined domains (see Supporting Information, Figure S8 and Tables S1 and S2).

Evaluation of the Recognition Ability of Thermoresponsive MIP

In this section, the selective recognition and selectivity of both MIPs were examined in the binding experiments. The α values determined the capacity of the imprinted polymer to distinguish between the isomeric compounds, compared to that for the respective reference materials (the control); enantioselectivity was denoted as the R/S enantiomer ratio. The deposited MIP showed a higher R/S enantiomer ratio and a more efficient enantiomeric release of the enantiomer print molecule from a mixture of the R/S enantiomers and individual enantiomer in MeOH at 37°C [Figure 6(A)]. Selectivity of the grafted polymer was similar to the deposited MIP except that there was an excess for the enantiomeric R/S ratio of 1 : 3 that showed a much lower selectivity value [see Figure 6(B)]. Moreover, a much smaller effect was observed for the individual enantiomers and the mixtures of the two enantiomers and the interactions between the pure enantiomer and both the MIPs had less effect at a lower pH (5.5) in an aqueous solution. At a higher pH (7.4, 8.0) the racemic mixture of thalidomide invariably showed differences between the racemate and the individual enantiomer. Thus, clearly, the inclusion of these compounds was spatially hindered by the (R)-thalidomide imprints, particularly in the physically adsorbed MIP particles.

Furthermore, the effect of temperature on the template binding to the grafted MIP from aqueous solutions during batch binding experiments was shown to be the best at 27°C [see Figure 6(B)]. At a higher temperature (37°C and 45°C), the imprint efficiency for the deposited polymerization was more significant than that for the grafted one, although that did exhibit a higher affinity and (R)-thalidomide enantioselectivity than did the corresponding NIP material in a pH 7.4 buffer solution. Also, the temperature dependence of the binding energy values of the deposited MIP has been found [see Supporting Information, Figure S9(a)], showing the linearity of the thermal generation of the recognition ability of the MIP-deposited nanoparticles. There was a clear linear dependency of the α values as a measure of the selectivity of the enantioselective binding site that appeared with an increase in the R/S ratio between the two enantiomers in the solution [see Supporting Information, Figure S9(b)]. Accordingly, this is the main effect of the temperature variations in the R/S enantiomeric ratio, but the magnitude of the enantiomeric ratio that appeared through the MIP system was dependent on the external stimuli. The observed differences indicated that stereospecific interactions occurred between the (R)-thalidomide and the MIP. However, the synthetic recognition materials achieved by the deposited polymerization process exhibited greater enantiomer discrimination than the grafted
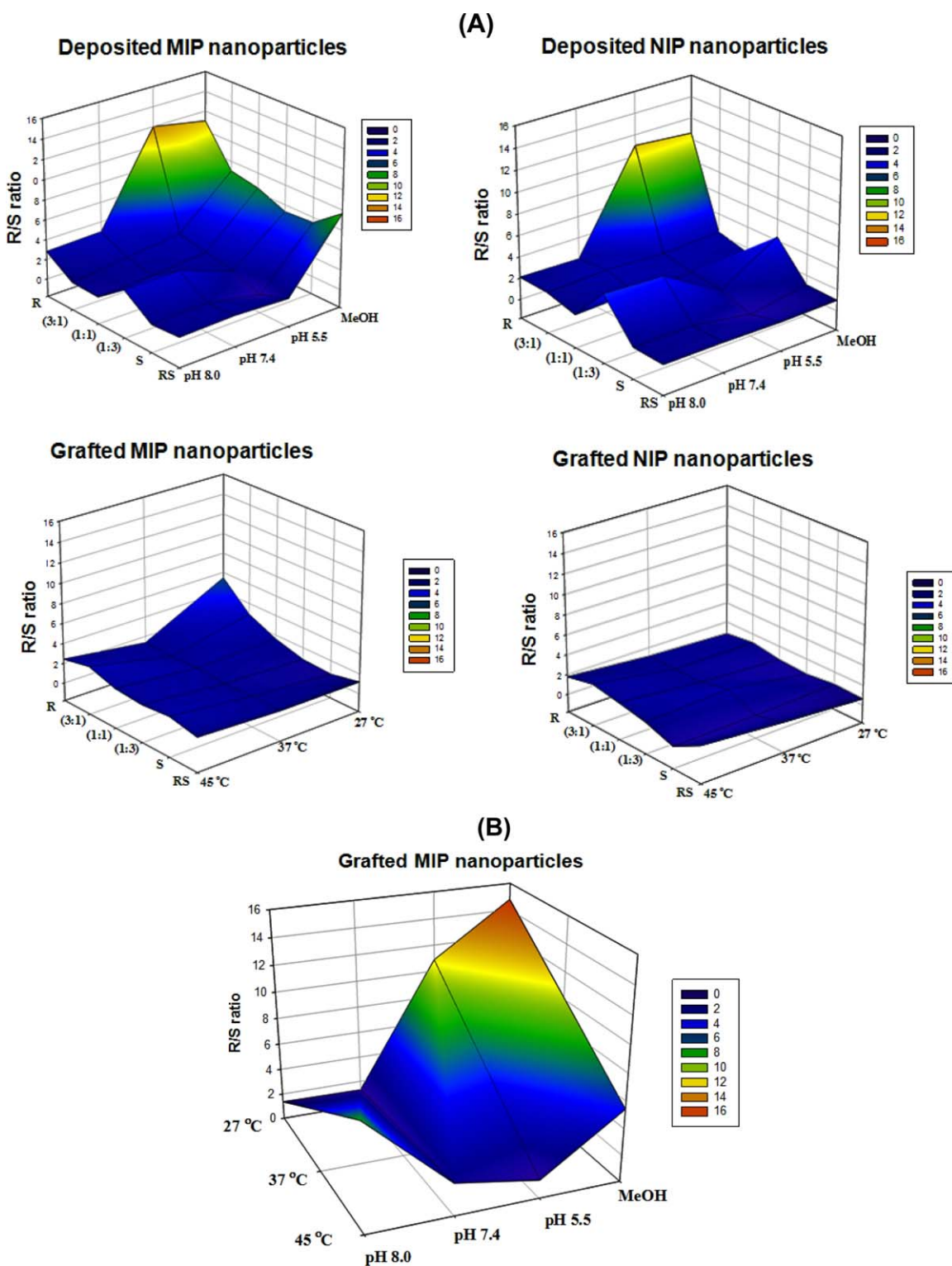
Figure 6. (A) The effect of the solvent media (top) and temperature (below) on the selectivity (R/S) of MIP and corresponding NIP nanoparticles when incubated with a single enantiomer or a racemic mixture, with the mixtures of the (R)- and the (S)-thalidomide enantiomers at ratios of 3 : 1, 1 : 3, and 1 : 1. (B) The 3D response surface plot showing effect of the solvent media and temperature on the selectivity (R/S) of the grafted MIP nanoparticles for (R)- and (S)-thalidomide at various ratios (mean $\pm$ SD, $n = 3$). [Color figure can be viewed in the online issue, which is available at wileyonlinelibrary.com.]

polymerization process at a higher temperature. The MIP provided them with hydrophobic interactions to form a complex with the nonpolar (R)-thalidomide. These interactions played

an important role in the binding process. The results have demonstrated that an MIP system can be prepared to provide affinity and specificity, with the ability to use complexation that

will, in general, vastly enhance its significance in the imprint effect.

The ^{1}H-NMR data gave linear plots between 27°C and 60°C. The difference between the chemical shift of the (R)-thalidomide in the presence of the deposited MIP in MeOH-d$_4$ changed by about 0.8 Hz K^{-1}. The least squares treatment yielded an equation for the MIP-deposited poloxamer nanoparticle:

$$T = 0.416 \ \Delta Hz - 112 [K].$$

The results obtained in this study have indicated that the thermal conductivity and capacitive behaviors provide useful insights into the interactions of a nematic system within the cross-linked networks that produce further benefits for the study of the recognition at a molecular level. Even a 1°C temperature difference is likely to affect the binding capacity of the drug to the binding site in the MIP. The determination of the adsorption capacities and processes of chirality of the MIPs with varying amounts of the (R)-thalidomide can be achieved by examining the differences of the free energy of the enantioselective binding of the deposited MIP. Therefore, all the data were used to calculate the enantiomeric ratio and the binding constant (K) using the Gibbs-Helmholtz equation:

$$\Delta\Delta G_{r,s} = -RT \ln \alpha_{r,s} = \Delta\Delta H_{r,s} - T\Delta\Delta S_{r,s}$$

where $\Delta\Delta H_{r,s}$ and $\Delta\Delta S_{r,s}$ represented the enthalpic and entropic component of the enantioselective binding, R is the gas constant of 1.987 cal mol^{-1} K^{-1} and T is the absolute temperature in Kelvin for the R and S enantiomers at the temperature being examined. The value of the association constant of the template enantiomer to the grafted-MIP was 0.925 M^{-1} at 27°C. The equilibrium constants for the formation of the activated complex by the deposited MIP, K_a at different temperatures were 0.24 M^{-1}, 0.83 M^{-1}, 1.61 M^{-1}, and 2.37 M^{-1} at room temperature, 27°C, 37°C, and 45°C, respectively. The binding constants of the enantiomeric ratios and the differences in the free energy ($\Delta\Delta G$) in the binding experiments for the deposited MIP nanoparticles at 37°C achieved in binding studies have been calculated to be ca. −2.75 kcal mol^{-1}. Furthermore, the dissociation of charged MAA functional groups of the MIP in an aqueous media results in the different numbers of the absorbed thalidomide at the binding site and the other nonselective material, which is usually described by a Boltzmann distribution [see Supporting Information, in eq. (S1)].

The observed changes in the experiment may have originated from a change in the affinity of the thermodynamic binding due to important conformational changes. Apparently, the topology of the interface became a major determinant for the adsorption capacity and affinity for both types of polymers. The dynamic motion of the pores along the polymer matrix involved rapid fluctuations of interconnected pores that were all about 30 nm in size (by TEM analysis), with an average of the internal radius pores of 10 nm and 5 nm. A quasi-steady state assumption q_d was assumed to occur across the boundary layer in the adjacent liquid medium, and the rate was linearly dependent on the temperature difference. In this way, the energy barrier can be calculated by the following equation:

$q_d = \kappa a (T_n - T_b) h$, where a, h, and $T_n - T_b$ are the area, height, and difference in the nanoparticle and the boundary temperatures. This allowed us to estimate the approximate pore migration using a perturbation expansion. When considering that the mobility of the internal pore was greater than that of the external pore dimension. The diffusion coefficient of the initial radius r was much less than the diffusion coefficient of the external radius R as the energetics of the pore formation and pore evolution were different, and thus the internal radius r and the external radius R would not be expected to become inserted into the polymer matrix. The nonstationary conduction (of diffusion) and the uniformly distributed points placed in contact with the medium were calculated by using a heating rate of the nanoparticles of 1.5×10^{-15} J s^{-1} and the imposing appropriate boundary; $a\nabla^2 T + Q = 0$. The energy barrier decreased when the deposited MIP, and the grafted MIP materials in the polymer matrix only increased the temperature of the poloxamer nanoparticles by 1.71×10^{-4} K or 1.01×10^{-6} K, respectively. Regardless of the heat balance in the polymeric material there was a different temperature distribution between the boundary layer and the center of the particle, the temperature of the covering area was assumed to be 37°C, so the analytical approximations to the pore dynamic were about 6.4×10^{-5} K and 1.1×10^{-4} K, for the deposited and grafted MIP nanoparticles, respectively. Thus, the deposited polymer had a lower energy barrier that inhibited the expansion and the pore quickly enlarged. Also, the electronic conductance of the physically adsorbed material, was determined by the calculation which was found to be 904/120.5 nH, and 1506.3/2410.3 nH, at 27°C and 60°C, respectively. The increase in the thermal conductance of the synthetic recognition material as a function of an elevated temperature was perhaps explained by the electronic polarization and was an alternative solution on the molecular electron-donor-acceptor complex of the assembled species via charge-transfer.[28]

The Stereoselective Release of the Thermoresponsive MIP Nanoparticle

Those who have examined the *in vitro* measurements of the nanocarriers involved in the controlled release of a desired drug, have shown that the rate of release was dependent on the physical properties of the synthetic polymer. Therefore, the total drug concentration within the particles decreased with time, but the drug concentration in solution around the particle remained essentially constant.[29] The characterization of the transport of the enantiomers from the source phase, across the organic layer, into the receiving solution at pH 5.5 for the (R)-enantiomer that was present in the racemic thalidomide revealed similar effects on the penetration of individual enantiomers [Figure 7(a)]. The difference in the enantiomer transferred into the receiving medium was much more pronounced with the addition of a single (R)-thalidomide [see Figure 7(b)]. However, some isomerization to the (S)-enantiomer occurred and diffused outward into the receiving phase from its periphery and the nonselective component. In Figure 7(c), a single (S)-thalidomide was added to a donor pH 7.4 solution and its penetration gradually increased, and as a result bidirectional inversion occurred that was strongly dependent on the contact time.
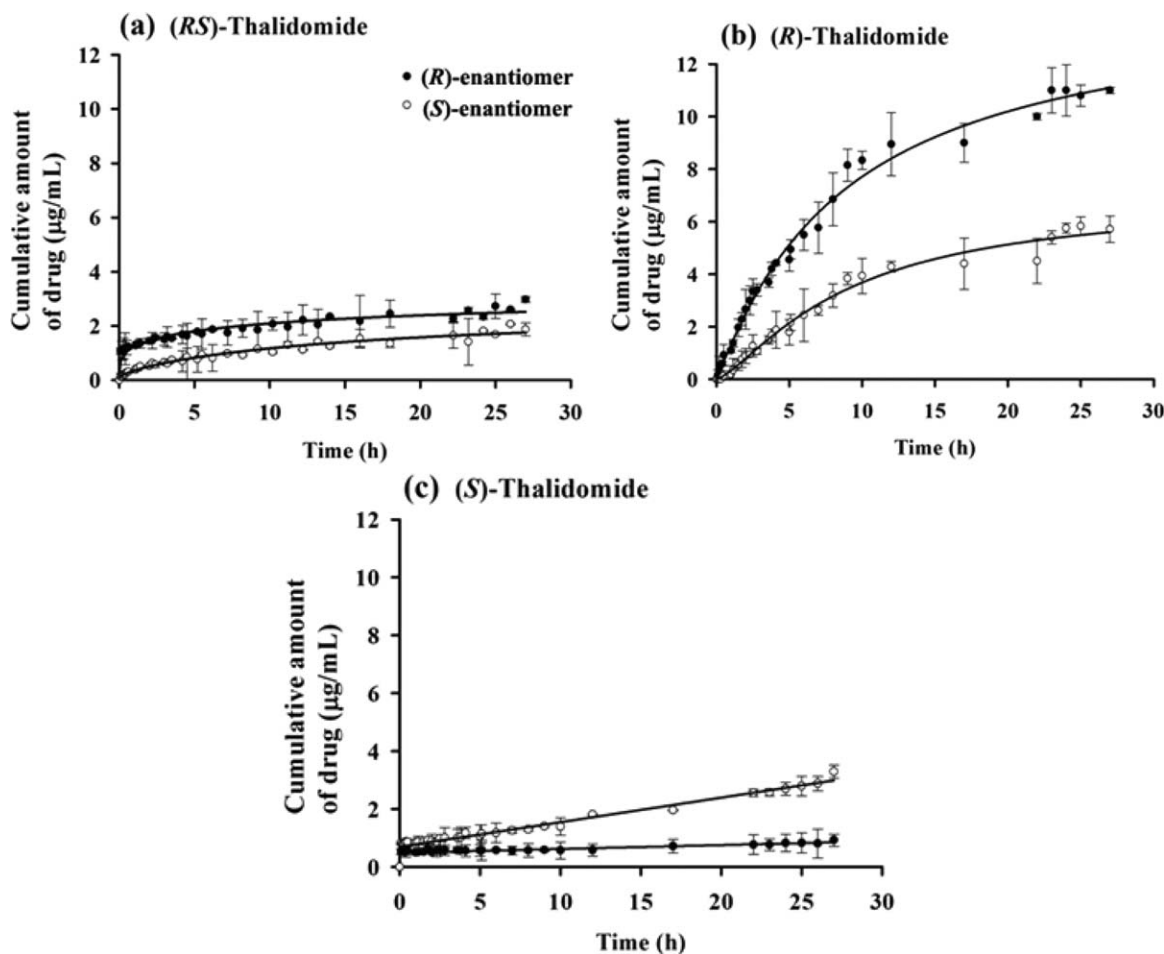
Figure 7. The release profiles of thalidomide enantiomers from a temperature-responsive nanocarrier embedded with: (a) (*rac*)-thalidomide; (b) (*R*)-thalidomide; and (c) (*S*)-thalidomide, at drug : polymer ratios of 4 : 1. The experiment was performed by applying pH 5.5 and 7.4 phosphate buffers in the donor and receiving phase, respectively, at 42°C (mean ± SD, $n = 3$).

Nevertheless, the penetration of the (*S*)-thalidomide enantiomer when added together with its racemate decreased to its lowest level but the penetration of the (*R*)-enantiomer remained almost unchanged over a 26 h period. The partition coefficient, K_c of the (*R*)-isomer increased and there was a significant difference found ($P < 0.01$) when loading either the (*S*)-thalidomide or the (*R*)-thalidomide into the liquid membrane (Table IV). For the racemic thalidomide, there was no significant difference in the K_c values of both isomers. This was attributed to

the stereoselectivity of the MIP and was also interpreted as the (*S*)-thalidomide being expected to compete equally with the (*R*)-thalidomide for the recognition cavity in the MIP that became saturated, and equally against the uptake of the (*S*)-thalidomide.

The selectivity of the device was consistent with the amount of the (*R*)-thalidomide MIP at the concentration that produced the IC_{50} (the concentration giving the 50% of penetration) as

Table IV. Partition, Binding Free Energy, and the IC_{50} for the (*R*)- and (*S*)-Thalidomide Enantiomers to a Model Liquid Membranes after Applying the MIP Nanoparticles and the NIP Nanoparticles Loaded with Different Chiral Target Species over a 26-h Period

Compound	K_c (µg L^{-1} min^{-1})		P value	F (s^{-1})		P value	IC_{50} (µg mL^{-1})		P value
	(*R*)-Isomer	(*S*)-Isomer		(*R*)-Isomer	(*S*)-Isomer		(*R*)-Isomer	(*S*)-Isomer	
Racemate	20.83 ± 3.65	15.62 ± 4.68	0.136	9.95 ± 0.54	9.89 ± 0.54	0.34	1.36 ± 0.31	0.95 ± 0.03	0.008
(*R*)-Thalidomide	117.18 ± 13.54	57.29 ± 5.21	0.002	292.30 ± 10.6	278.06 ± 26.8	0.27	5.86 ± 1.13	2.89 ± 0.32	0.01
(*S*)-Thalidomide	8.33 ± 3.12	32.29 ± 2.08	0.001	266.49 ± 0.38	272.41 ± 1.11	0.005	0.34 ± 0.04	1.66 ± 0.12	0.0001

Each value represents the average of four independent measurements for all of polymers.
Statistically significant different of (*R*)- and (*S*)-thalidomide enantiomers ($P < 0.05$).

Table V. The Drug Release Behaviors of the Thalidomide Enantiomers When 2 mg of Racemic Thalidomide Transport into Water/Chloroform Interface Containing of the MIP and NIP Nanoparticles Loaded With (R)-Thalidomide (1 : 4 Drug Polymer Mixture) After a 96-h Dissolution Process

Polymer	In donor aqueous suspension (μg)			Zero order slope (μg min^{-1} cm^{-2})			Plateau value (μg cm^{-2})			Rate constant (10^{-3} ms^{-1})		
	(S)-Isomer	(R)-Isomer	P value	(S)-Isomer	(R)-Isomer	P value	(S)-Isomer	(R)-Isomer	P value	(S)-Isomer	(R)-Isomer	P value
MIP	15.48 ± 4.75	18.43 ± 5.30	0.439	0.078 ± 0.008	0.089 ± 0.004	0.049	56.41 ± 3.00	99.84 ± 6.15	0.001	0.250 ± 0.013	0.376 ± 0.015	0.001
NIP	17.08 ± 3.90	18.01 ± 5.59	0.794	0.089 ± 0.005	0.092 ± 0.004	0.385	76.47 ± 2.88	78.24 ± 3.40	0.457	0.345 ± 0.013	0.360 ± 0.015	0.181

Mean $\pm$ SD, $n = 4$.
Statistically significant different of (R)- and (S)-thalidomide enantiomers ($P < 0.05$).

shown in Table IV. The distinctly different IC_{50} values between the individual thalidomide enantiomers and the racemate can be explained in that to some extent, through the three dimensional structures and orientations of the molecules in the racemic mixtures that were invariably different from the templating species. The MIP system exhibited the highest IC_{50} with the (R)-thalidomide. When the equimolar mixture of both enantiomers was added, the differences of the IC_{50} values in all the cases were found to be statistically significant. Either the racemate or the (S)-enantiomer fitting into the (R)-isomer imprint was spatially intrinsically inaccessible at a spatially ill-defined cavity. For the racemate into a solution that contained one of the two enantiomers, a remarkably different binding from that for the pure enantiomer, and a remarkably lowered energy orientation than those of the pure enantiomer were observed (see Table IV). The racemate exhibited a distinct minimum in the free energy for both enantiomers. The addition of a single (R)-thalidomide indicated free energies of interaction very similar to those of the (S)-thalidomide, however, the addition of the pure (S)-enantiomer led to the observed statistical differences between the two isomers. The differences in free energy between the two chiral molecules were not caused by the favored adsorption of the (R)-thalidomide imprint. While the racemic mixture of the thalidomide exhibited significant differences in the interaction of both enantiomers with the MIP, it was found that the matrix hydration led to free diffusion of a chiral molecule in the composed material. The behavior of the (S)-form of the thalidomide resulted in a reduced configurational conversion to the (R)-form following transport with the MIP. Taken together, these results provide strong evidence that the imprinted nanoparticles prevented the conversion of the thalidomide enantiomers, which supports the existence of intermolecular interactions of the molecular chiral species and the binding site in the MIP/poloxamer nanoparticles at the water/chloroform interface.

In this study we confirmed that at the interface of the first site of contact, the thermodynamics for insertion of the nonconstitutive substances that consisted of the (R)-enantiomer of thalidomide had little effect. Table V shows the drug release behaviors of 2 mg of the racemic thalidomide that was added in the donor phase. The addition of the (R)-thalidomide enantiomer and the racemic thalidomide to the MIP and the corresponding NIP control polymer led to the difference in the zero-order slope of the enantiomer being virtually modest. The MIP-deposited nanoparticles demonstrated a 1 : 4 ratio of selectivity and the amounts of the (R)-enantiomer were higher than the (S)-enantiomer (see Supporting Information, Figure S10). The results indicated that the rate constants to the first approximation would be expected to be not solely dependent on the interaction between the enantiomer and the nanoparticles. For the NIP, there appeared to be no difference of the rate constant values of both the enantiomers because there were no specific interfacial sites on the nanoparticles for the target to be incorporated. In addition, the time required for a steady-state equilibrium for binding was about 12 h, following the point where the matrix was brought into contact with the release media. The differences in the steady-state rates were found to be statistically significant (P value $= 0.001$, for all the cases). This

response time correlates to the time the binding needs to reach equilibrium, which in turn is dependent on two means, the diffusion of the template from the bulk solution through the pores to the binding cavities and the actual binding kinetics between the template and the cavities. A determination of the concentration of a single enantiomer of the thalidomide to add to the solution, with a sensitivity of up to 10 μg mL^{-1} and had the ability to detect changes in the concentrations over a range of 2–12 μg mL^{-1}. The MIP-deposited nanoparticles showed a higher apparent binding capacity (3.1 μmol g^{-1}) than the MIP-grafted nanoparticles (1.1 μmol g^{-1}). The MIP-grafted material bound the (R)-thalidomide approximately one order of magnitude less tightly than the deposited MIP ($K_a = 0.11$ vs. 1.02 M^{-1}). This selectivity was related to characteristics of the recognition cavities that had been imprinted on the poloxamer nanoparticles to provide for a high concentration of the template-MIP complexes in the polymer matrix. As a result a significant numbers of template binding sites, which were manifested by an enhanced rebinding efficiency. The solid-liquid interfaces of the nanoparticles-bound to the receptor mimic produced an interaction of a surface-mirrored polymer in the cross-linked chains was compared, for determining the original properties of the (R)-thalidomide. The rate constant of the transport between the two enantiomers were found to be significantly different, in which the rate of the (R)-enantiomer ($0.376 \pm 0.015\ 10^{-3}$ ms^{-1}) was higher than that of the (S)-enantiomer ($0.250 \pm 0.013\ 10^{-3}$ ms^{-1}). In addition the steady-state rates and the rate constants towards the two thalidomide enantiomers were found to be statistically significantly different (P value = 0.001, for all the cases). The results of the enantioselectivity and penetration at the lipid bilayer interface showed that changing the external temperature led to a selective release. The complex was formed between the functionalities of the template and the functional monomers for both the MIPs that were supported by producing a molecular model.[30,31] Figure 8(a) showed the structure and the optimized geometry of both the MIPs at a lower temperature (298 K). At 310 K, the cavity and the molecular surface of the deposited MIPs that a three dimensional structure model obtained was compared to the MIP at 318 K [Figure 8(a)]. The grafted MIP contained the surface imprinted sites that enabled it to embrace the surface properties of the (R)-thalidomide at 298 K, as shown in Figure 8(b), and at 318 K. There are possible racemizations and degradation of the thalidomide enantiomers in a solution. As seen in Figure 8(c), the energy profile by the computer simulations confirmed that the free energy barrier of 2-hydroxyl thalidomide intermediate was the lowest free energy as compared to the structure of the two enantiomers. It has been shown in the current study that the hydroxylated thalidomide was presumably formed that was reduced as well as the reduced bidirectional conversion of the enantiomers in the nanoparticles when exposed to the pH 7.4 buffer at 42°C. The half-life for the degradation of the thalidomide in the aqueous medium at physiological pH was examined through this approach and was found to be 5.75 ± 1.0 h. In an acidic medium (pH 5.5), thalidomide was protected from hydrolysis, and both enantiomers remained.

By using a detector with a built-in thermoresponsive MIP, it was anticipated that it could be applied as a method for sensing

and diagnostics for biological applications. As shown in Figure 9(A), the AFM images of the pyridinium-based MIP, embedded in a poloxamer nanoparticle were examined using varying the solvents. The nanomaterial in acetone or a mixture of acetone and IPA showed clusters of oriented MAA-BAAP bound to the MIP in AFM image. There appeared to be small pillars of the material in the acetone and IPA mixture in the AFM image with a nanosized scale of spatial resolution on the assemblies that confirmed the close packing density of the MIP binding sites in the confined nanoparticles.[32] It was evident that the fluorescence emission and excitation peaks were present at a different medium pH [Figure 9(B)]. The 2D-FEEM spectra were apparently different from those of the MIP of the deposited version at a pH of 7.4 and after exposure to a pH 5.5 buffer solution. Observation on the tunable fluorescence spectra, especially for several excitation (200–300 nm) and emission (200–500 nm) wavelength values, are shown in Figure 9[B(a)] and a distinctly different spectral region for the deposited NIP at the two pH values is shown in Figure 9[B(b)]. It was surprising that the MIP-deposited nanoparticle as most readily observable fluorescence emission at pH 7.4 only, and this presented as a continuation of the fluorescence emission at several excitation wavelengths. In contrast, in Figure 9[B(c,d)], the MIP-grafted nanoparticles provided a continuation of the fluorescence emission at only one excitation wavelength of approximately 300 nm at pH 7.4. This was advantageous for producing an unprecedented clean quantum structure. The confinement of the charged excitations that were fabricated by the intrinsic fluorescence characteristics of the carbonyls and pyridines of the BAAP functional group inside a spatially restriction region appeared to be a pH-triggered controlled quantum fluorescence emission. This was conceivably attributed to the MIP because of photoexcitation, an exciton was formed and allowed an electron to be promoted with a charge migration to occur as an electron jump. However, during the fluorescence, a photon was emitted when the valence electrons were excited and led to the relaxation into the ground state. As a consequence the most important properties were a change in the active fluorescent group in the BAAP-bound cavity on its fluorescence emission. However, the energy of the photon was equal to the band gap that depended on the topography and an environmentally sensitive property of an MBAA-crosslinked polymer surrounding the block copolymer of the poloxamer. Additional evidence that supported this charge transfer complex was confirmed by the crystals that formed in a pale emerald-green colored solution during the prepolymerization and that remained only in the MIP grafted nanomaterial.

Furthermore, the effect of smaller sized molecules led to the optoelectronic properties of the poloxamer nanoparticle that consisted of the poly(MBAA) crosslinked chains surrounding the MIP in the mixture of acetone and IPA, which showed dimensional spaces in the order of only 60 nm [Figure 9(C)]. When feeding daphnia, with the organic electronic material, the reduction of the particle size of the nanomaterials made possible by the deposited MIP nanoparticles demonstrated a microcirculation in the body with penetration of the visible polymers under UV (366 nm). These were distributed throughout the
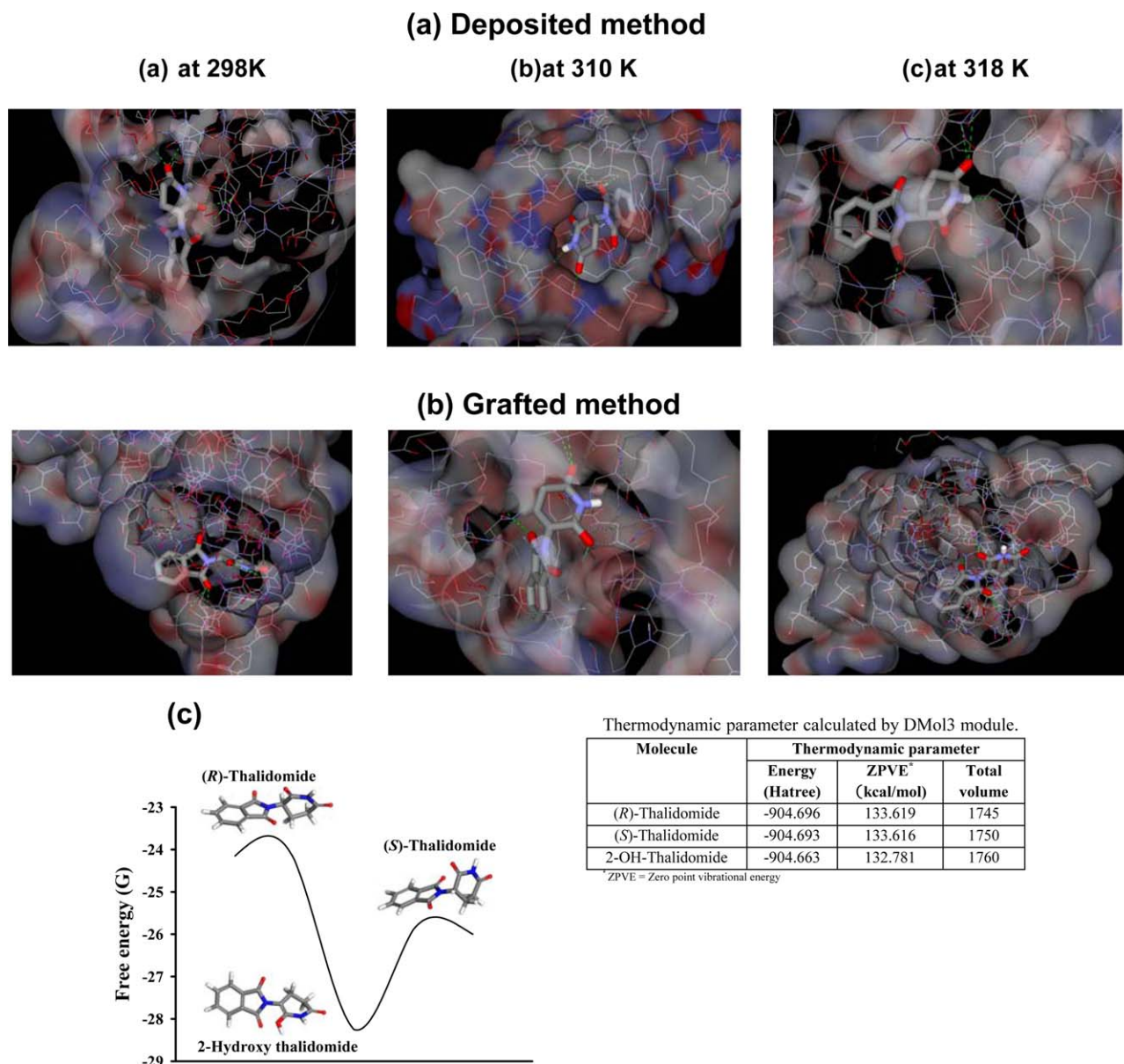
Figure 8. The computer simulations depict the intermolecular contacts in the imprinted cavities at 298 K, 310 K, and 318 K: (a) the deposit method, (b) the grafting method, after reaching equilibrium in the MD simulation. In all panels, hydrogen-bonding interactions are represented by green dashed lines. (c) Free energy profile for the inter-conversion of individual structures of the thalidomide enantiomers through 2-hydroxyl thalidomide intermediate molecule in water (insert: thermodynamic data calculated by DMol3 module). [Color figure can be viewed in the online issue, which is available at wileyonlinelibrary.com.]

body immediately after application and were bound to the daphnia gut cell membranes and other cell surfaces, to indicate that the nanomaterial was biocompatible and nontoxic.

The intracellular localization at the right edge of the MIP nanoparticles with the loaded drug was of interest as it was fused to an apparent increase in intensity of the green fluorescence in the presence of the racemic thalidomide. The fading of this fluorescent nanoparticle occurred within 28 h. Although NIP controlled polymers produced the green fluorescence of the nanoparticle, in Figure 10(a) exhibited focal adhesion and orientation in cancer cells when no cell cytoskeletal distortion was

observed [Figure 10(b)]. Either of the MIP nanoparticles appeared in the green fluorescence [Figure 10(c)] and the CLSM images of the individual cells showed a rough and round morphology, and they could extend around the MIP poloxamer nanoparticles look like "ring" [Figure 10(d)]. The results of the cell culture revealed the mobility of the poloxamer nanocomposite material embedded on cancer cell-adhering surface resulting in physical and mechanical properties of the cancer cell and the surface chemistry of MIP within the microenvironment, therefore providing the cytotoxic mechanism of the nanoparticles. This was unlike the cancer cell without treatment [Figure 10(e)], which remained small, and these cells appeared to have
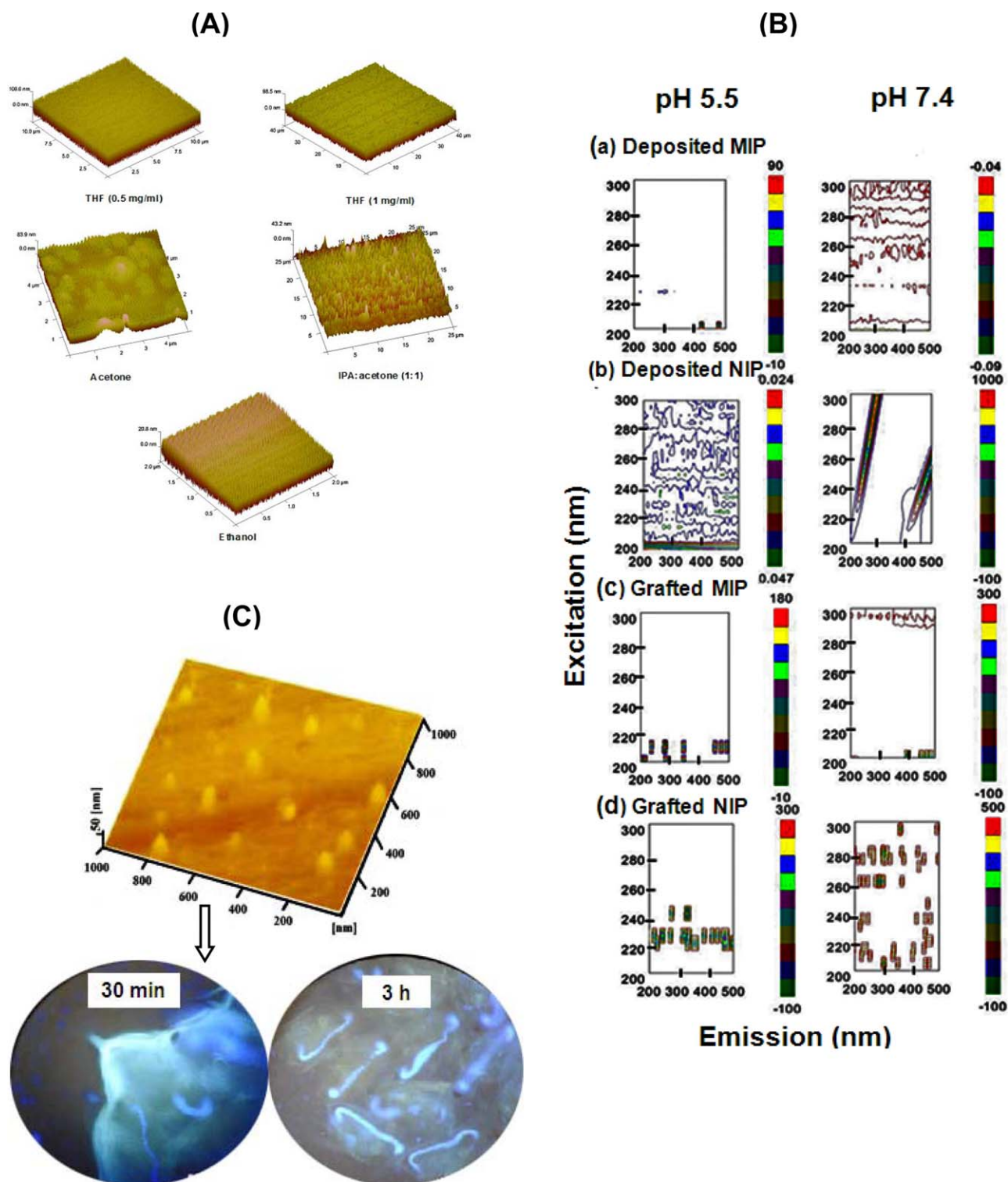
Figure 9. (A) The AFM image of the MIP/poloxamer nanoparticles in ethanol, THF, acetone and IPA and the mixture of acetone and IPA after being dispersed in 1 : 1 IPA/acetone mixture. (B) A 2D-*FEEM spectra showing the t*unable fluorescence of *(a)* the *deposited MIP nanoparticles;* (b) the corresponding NIP in the pH 7.4 solvent after several excitations (200–300 nm) and the emission (200–500 nm) wavelength; (c) a continuation of the fluorescence emission of the MIP-grafted nanoparticles showing only one excitation wavelength of approximately 300 nm at pH 7.4, and (d) the control polymer provided a fluorescence emission at a particular excitation wavelength measured at either of the pH 5.5 or 7.4 values. (C) Microscopic imaging of uptake in *Daphnia longispina* (waterflea) of the MIP-deposited poloxamer nanoparticles, which showed dimensional spaces in the order of 60 nm showing effect of reducing smaller molecular size on the optoelectronic properties of MIP-deposited poloxamer nanoparticle under UV light. [Color figure can be viewed in the online issue, which is available at wileyonlinelibrary.com.]
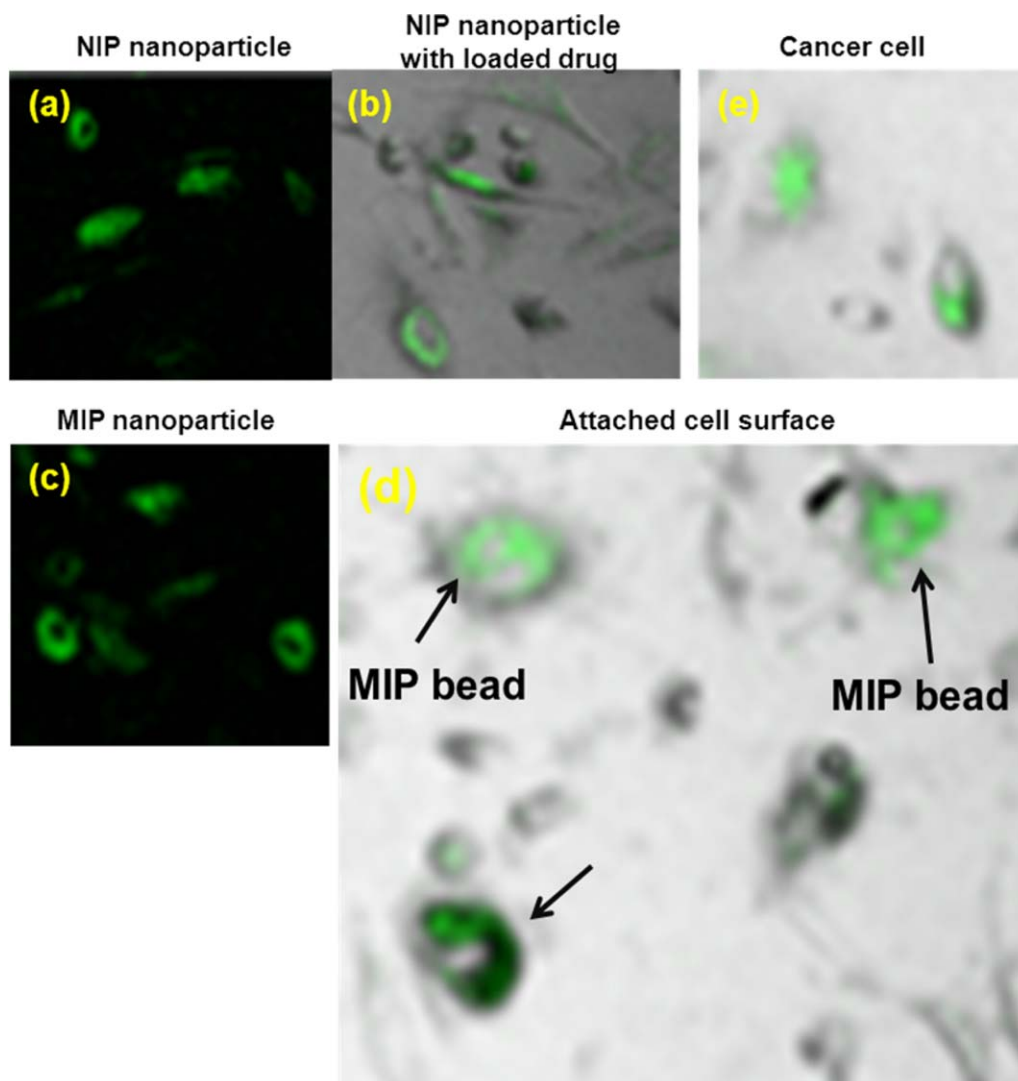
Figure 10. Fluorescence of induced cancer cell cultures. (a) Fluorescence images of the NIP without and (b) with the loaded racemic thalidomide in the cancer cells and (c) MIP nanoparticles alone. (d) A bright-field and fluorescence images of the racemic thalidomide-loaded MIP nanoparticles showing focal adhesion and orientation with a cell cytoskeletal distortion at the top right of the view and appears as a green crescent on the right edge of the MIP nanoparticle at the bottom left of the view (arrow). (e) A blank cancer cell is given for comparison (all images at a magnification of 40×). [Color figure can be viewed in the online issue, which is available at wileyonlinelibrary.com.]

a flattened nucleus. In Figure 11, cancer cells transformed with the MIP-loaded thalidomide construct showed a larger distribution of fluorescence after 28 h and there was a bigger effect on the green fluorescence (a 1.5-fold increase in the fluoresce for the deposited MIP with respect to the NIP as compared to a fourfold increase for the grafted MIP). In contrast, the fluorescent intensity ratio of the corresponding NIPs that was introduced, either with or without the drug, barely changed. In addition, there were different green fluorescent intensities between those of the loaded drug and the nonloaded drug that appeared with the grafted MIP (statistically significant, $P < 0.05$). In contrast, the distribution of the fluorescence by the deposited MIP and its corresponding NIP was insignificant. Indeed, the generation of the oriented motion, caused geometric changes in the aggregated particle (0.025 Ns m^{-2} and 0.0035 Ns m^{-2} for the dry and liquid state, respectively) as evaluated from

the hydrodynamic particle size in MeOH.[33] Hence, the latter polymer did not form an intimate contact at the interface because of the flexibility of the polymer chains and the dramatic changes in the viscosity of the nanoparticles, and as such the energy dissipation was smaller. Obviously, the distribution of the fluorescence of the MIPs was significant with respect to fluorescence in the cell, as well as to the association of the drug to the protein a binding that was specifically expressed in the cancer cells that caused an extension of the green fluorescence intensity. Besides, the difference in nonspecific adsorption of two MIPs concerned with the measured fluorescence intensity was caused by having a template with a complementary nonfavorable functionality. Differences in the nature of the vehicle, the microscopic structures, and the construction of a gel network to the nanoparticles will, however, affect the physical features and the fluorescence emissions of the obtained devices. With the
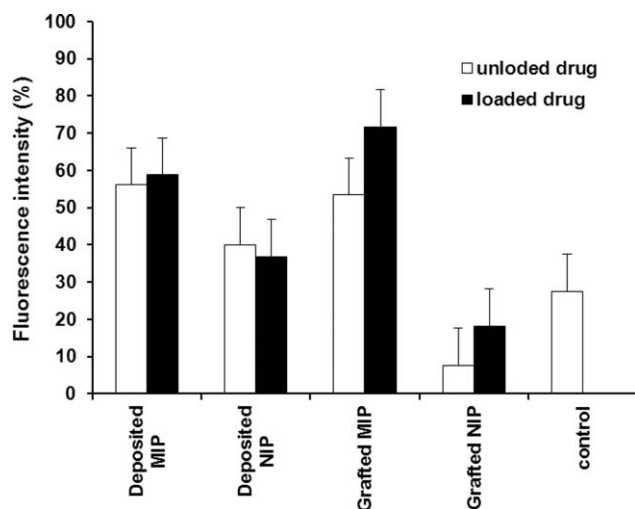
Figure 11. Plot of the percentage of the green fluorescent intensity generated by incubating the NIP and MIP nanoparticles with and without racemic thalidomide in the cell cultured system for 28 h in the standard culture media. For each sample, the fluorescence level of the induced cancer cell cultures was compared with a control cancer cell line.

results obtained, the less nonspecific property of the grafted material and the complexes of the drug and the chiral MIP were achieved from the measurement of the intensity of the spectroscopic fluorescence that resulted in the alteration to the template rebinding to the accessible sites, and led to the release of the template within the BAAP-bound cavity in the MIP under the surrounding extracellular environment. The effect of

the increased migration of cancer cells due to the increased TNF-α level produced in a cell line or in myeloma cells has been previously reported.[34] These findings indicate that the binding of the enantioselective receptor to the thalidomide enantiomer that altered in protein expression strongly supported the view on TNF-α association to the domain mediated signal for an increase in the intensity of the green fluorescence.

As shown in Figure 12(a,b) when the human cancer cells were treated with the racemic thalidomide incubated either with or without the deposited-MIP only the one that provided for the (R)-thalidomide affected the proliferation of the cancer cell and its migration after 24 h. In Figure 12(c), it can be seen that the cancer cells treated with thalidomide alone showed no change in the morphological characteristics of the cancer cell. The MIP or the NIP and the loaded thalidomide clearly displayed a change in cell shape, and showed long tails in contrast to the control cancer cell-line [see Figure 12(e,f)]. However, the respective NIP did not result in an effective functional activity any further, than those for the MIP [Figure 12(d)]. More importantly, the advantage of the chiral MIP receptor and the loaded thalidomide was the cell imaging by exposure to UV light that could lead to the cancer cell lysis [Figure 12(g)] and the aggregation of cells and even DNA breakages [Figure 12(h)] could be clearly observed. Accordingly, the finding that a more sensitive and bigger response of the biological process in the cancer cell appeared because of the ability of the (R)-thalidomide imprinted polymer to become an accessible target binding site would indicate that the cancerous cell conditions decreased the binding events of the thalidomide imprint and enhanced
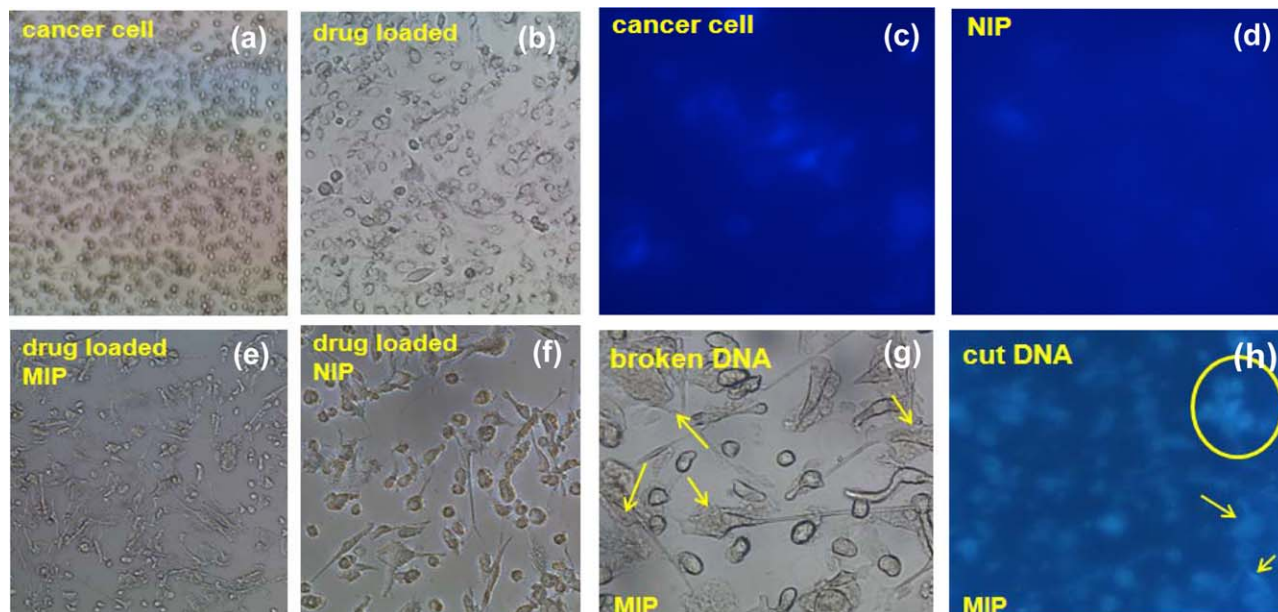

Figure 12. Light microscope image at 10× magnification showing human adenocarcinoma epithelial cell line (a) in culture medium before UV light exposure, (b) incubated with thalidomide for 24 h showing several nuclei within the cells, (c) after the UV exposure for 1 min, and (d) after incubation with the NIP loaded thalidomide. (e and f) A microscope image (40× magnification) of the cancer cells after incubation with the MIP and NIP nanoparticles showing the long tails of the cells and (g) the increased interaction of thalidomide in the cancer cell lines exposed to the MIP nanoparticle, leading to broken DNA. (h) The fluorescent images of the MIP to proteins during UV light exposure. Circle: a selected nucleus of the aggregated cells is marked. Arrowheads point to the DNA damage sites before a DNA break after exposure to UV light. [Color figure can be viewed in the online issue, which is available at wileyonlinelibrary.com.]

the efficiency of the template rebinding. On the other hand, for the NIP, there appeared to be no difference of the UV responses within the cells which confirmed that the chirally imprinted polymer served for sensing, or monitoring the MIP as an optically fluorescence biosensor, without compromising the desired biological activity.[35] These data indicate that the template was effectively inserted into the chirally molecular imprinted polymer receptor of the nanoparticle (which did not give fluorescence emission) and was linked to the optoelectronic properties in the fluorescently active BAAP-bound imprint cavity. It is intriguing that a thermostimulated material that could release the drug inside the cancer cells can now be readily observed. This result shows good promise for finding composite nanomaterials in the presence of (R)-thalidomide that could be assimilated by the multiresistant cultured cells that were caused by the association of an enantioselective receptor that they can kill the cancers with the thalidomide loaded MIP nanoparticles. Taking together, these results support the view that the differences of the confined surface structures and the spaces within the poloxamer nanoparticles could be distinguished to reflect the cancer drug activity of the bound template in the differences of the recognition cavity between the two different polymerization processes.

CONCLUSIONS

In this study, MIPs for (R)-thalidomide were synthesized to bind biological ligands using the means of the preorganization of the polymerizing mixture that consisted of mixed functional monomers, a crosslinking agent and poloxamers, which together resulted in the prepolymerized mixtures structured with the template (R)-thalidomide. Obviously, the benefit of poloxamer nanoparticles containing fluorophores from the functional monomer BAAP as the component of the molecularly imprinted polymer was found to be very useful for a high thermodynamic binding efficiency and a sensitive, precise self-reporting element. This process can be easily modified and expanded by using different templating targets such as for other pharmaceutically active chiral drugs. In the case described above, the recognition material prevented (R)-thalidomide from racemization and, therefore, overcame putative differences in therapeutics or the adverse effects of the opposite enantiomer due to the rapid interconversion of the enantiomers *in vivo* that were now, to a large extent abolished. The selective materials have a high potential for detecting different cell stages from the effect of the fluorescence emissions, and enabled a check-up on the progression of the treatment that could provide, especially for the detection of a noninvasive disease, a situation that is desperately required for cancer research. An alternative advantage for using such recognition materials within poloxamer nanoparticles appeared to be the ability to penetrate and localize the drug to cause apoptosis in a multidrug-resistant model with a potential use as an anticancer agent on drug resistant cells. An MIP in a temperature-sensitive nanocarrier may be utilized as means for chiral recognition and the selective release of the drug in response to a temperature stimulus, thus enabling the desired enantiomer to be delivered to the targeted site with maximum efficiency.

REFERENCES

1. Mujahid, A.; Dickert, F. L. In Supramolecular System in Biomedical Fields; Schneider, H., ed; RCS Publishing, Thomas Graham House Science Park: Cambridge, **2013**; p 419.

2. Iqbal, N.; Mustafa, G.; Rehman, A.; Najafi, B.; Lieberzeit, P. A.; Dickert, F. L. *Sensors* **2010**, *10*, 6361.

3. Schirhagl, R.; Lieberzeit, P. A.; Dickert, F. L. *Adv. Mater.* **2010**, *22*, 2078.

4. Hoshino, Y.; Kodama, T.; Okahata, Y.; Shea, K. J. *J. Am. Chem. Soc.* **2008**, *130*, 15242.

5. Mosbach, K.; Yu, Y.; Andersson, J.; Ye, L. *J. Am. Chem. Soc.* **2001**, *123*, 12420.

6. Suedee, R.; Srichana, T.; Rattananont, T. *Drug Del.* **2002**, *9*, 19.

7. Jantarat, C.; Tangthong, N.; Songkro, S.; Martin, R.; Suedee, R. *Int. J. Pharm.* **2008**, *349*, 221.

8. Leopold, K. A.; Dewhirst, M.; Samulski, T.; Harrelson, J.; Tucker, J. A.; George, S. L. *Int. J. Radiat. Oncol. Biol. Phys.* **1992**, *22*, 989.

9. Hattori, Y.; Iguchi, T. *Congenital Anomalies* **2004**, *44*, 125.

10. Eriksson, T.; Björkman, S.; Roth, B.; Fyge, Å.; Höglund, P. *Chirality* **1995**, *7*, 44.

11. D'Amato, R. J.; Loughnan, M. S.; Flynn, E.; Folkman, J. *Proc. Natl. Acad. Sci. USA* **1994**, *91*, 4082.

12. Rossi, S.; Kyne, G. M.; Turner, D. L.; Wells, N. J.; Kilburn, J. D. *Angew Chem. Int. Ed.* **2002**, *41*, 4233.

13. Rosenger, J. P.; Karlsson, I. G.; Nicholls, I. A. *Org. Biomol. Chem.* **2004**, *2*, 3374.

14. Kono, K.; Henmi, A.; Takagishi, T. *Biochim. Biophys. Acta* **1999**, *1421*, 183.

15. Pastuszka, M. K.; Janib, S. M.; Weitzhandler, I.; Okamoto, C. T.; Hamm-Alvarez, S.; Mackay, J. A. *Biomacromolecules* **2012**, *12*, 3439.

16. Tauer, K.; Weber, N.; Texter, J. *Chem. Comm.* **2009**, 6065.

17. Hussain, M.; Wackerlig, J.; Lieberzeit, A. P. *Biosensors* **2013**, *3*, 89.

18. Schirhagl, R. *Anal. Chem.* **2014**, *86*, 250.

19. Bae, Y.; Fukushima, S.; Harada, A.; Kataoka, K. *Angew Chem. Int. Ed.* **2003**, *42*, 4640.

20. Grossiord, J. L.; Dumortier, G.; Agnely, F.; Chaumeil, J. C. *Pharm. Res.* **2006**, *23*, 2709.

21. Kabanov, A. V.; Batrakova, E. V.; Sriadibhatla, S.; Yang, Z.; Kelly, D. L.; Alakov, V. Y. *J. Control. Release* **2005**, *101*, 259.

22. Hoffman, A. S. *J. Control. Release* **1987**, *6*, 297.

23. Oikawa, E.; Motomi, K.; Aoki, T. *J. Polym. Sci. Part A: Polym. Chem.* **1993**, *31*, 457.

24. Lyon, A. W.; Duran, G.; Raisys, V. A. *Lin. Biochem.* **1995**, *28*, 467.

25. ICH Harmonized tripartite guideline, Validation of analytical procedures Q2(R1), Current step 4 version, Geneva, 2005.

26. Chizmadzhev, Y. A.; Cohen, F. S.; Scherbakov, A.; Zimmerberg, J. *Biophys. J.* **1996**, 2485.

27. Walter, J.; Sehrt, J.; Vrabec, J.; Hasse, H. *J. Phy. Chem. B* **2012**, *116*, 5251.

28. Suedee, R.; Intakong, W.; Dickert, F. L. *Anal. Chim. Acta* **2006**, *569*, 66.

29. Chan, A. F.; Evan, D. F.; Cussler, E. L. *AIChE J.* **1976**, *22*, 1006.

30. Torimoto, N.; Ishii, I.; Hata, M.; Torimoto, N.; Ishii, I.; Ariyoshi, N.; Ohmori, S.; Igarashi, T.; Kitada, M. *Biochemistry* **2003**, *42*, 15068.

31. Yarovsky, I.; Evans, E. *Polymer* **2002**, *4*, 963.

32. van Hemelrijck, Muller-Goymann, C. C. *Int. J. Pharm.* **2010**, *420*, 297.

33. Kötitz, R.; Fannin, P. C.; Trahms, L. *J. Magn. Magn. Mater.* **1995**, *149*, 42.

34. Jöhrer, K.; Janke, K.; Krugmann, J.; Fiegl, M.; Greil, R. *Clin. Cancer Res.* **2004**, 10, *1901*.

35. Wong, B. M.; Lee, J. W. *J. Phys. Chem. Lett.* **2011**, *2*, 2702.